TRENDS IN SCIENCES 2026; 23(9): 13253
https://doi.org/10.48048/tis.2026.13253
REVIEW ARTICLE

Recent Advances in $MnFe_2O_4$/Activated Carbon Composites for Environmental and Energy Applications: A Comprehensive Review on Synthesis, Characterization, and Performance

Dinda Amilia[1], Noor Haida Mohd Kaus[1,*] and Muhammadin Hamid[1,2]

[1]*School of Chemical Sciences, Universiti Sains Malaysia, Pulau Pinang11800, Malaysia*
[2]*Department of Physics, Universitas Sumatera Utara, Medan 20155, Indonesia*

([*]Corresponding author's e-mail: noorhaida@usm.my)

Received: 3 January 2026, Revised: 21 February 2026, Accepted: 1 March 2026, Published: 10 April 2026

Abstract

$MnFe_2O_4$/activated carbon composites have emerged as multifunctional materials that combine the catalytic and magnetic properties of manganese ferrite with the high surface area, porosity, and chemical stability of activated carbon. Structural characterizations confirm the successful formation of crystalline spinel $MnFe_2O_4$ phases uniformly dispersed within the carbon matrix, enhancing stability and reducing nanoparticle agglomeration. These composites exhibit outstanding adsorption and photocatalytic efficiencies, achieving high removal rates for pesticides, antibiotics, nutrients, and aromatic organics, while showing promise for microwave absorption, electrocatalysis, and energy conversion. Waste-derived activated carbon precursors, such as coconut shells, coffee husks, and durian peels, further improve sustainability and cost-effectiveness, aligning with circular economy principles. Mechanistic studies reveal synergistic pollutant removal: $MnFe_2O_4$ provides redox-active sites and magnetic recovery, while activated carbon offers functional groups, facilitates electron transfer, and mitigates charge recombination. Despite these advantages, challenges persist in scalability, long-term regeneration, and real-world applications in complex wastewater matrices. Future work should prioritize green, scalable synthesis, pilot-scale trials, and hybrid treatment systems to translate $MnFe_2O_4$/activated carbon composites into practical environmental and energy technologies.

Keywords: $MnFe_2O_4$/activated carbon composites, Activated carbon, Manganese ferrite, Adsorption, Photocatalysis, Wastewater treatment, Sustainable synthesis, Multifunctional materials

Introduction

The release of persistent and bio accumulative pollutants has become a critical environmental and public health concern. Many industrial contaminants, particularly those originating from textile and pharmaceutical activities, are toxic, poorly biodegradable, and resistant to conventional treatment methods, leading to long-term ecological damage and severe health risks such as metabolic disorders, cancer, and cardiovascular diseases [1-3]. The exposure to human occurs through multiple pathways, including inhalation, ingestion, and dermal contact, further amplifying the global health risks [4]. These challenges highlight the urgent need for sustainable water treatment technologies that are capable of efficiently removing recalcitrant pollutants while minimizing the secondary environmental impacts [5].

Among the existing approaches, adsorption has been widely applied because of its simplicity, cost-effectiveness, and capability for removing a broad range of contaminants [6]. However, the limitations related to adsorbent regeneration and secondary waste generation often restrict their long-term applicability. Therefore, photocatalysis has therefore emerged as a promising green alternative because it utilizes solar energy to reduce the persistent pollutants into less harmful products [7,8]. Nevertheless, many conventional treatment techniques, including coagulation, membrane

filtration, and biological processes, remain energy-intensive, inefficient for refractory pollutants, and associated with secondary sludge formation [9]. Nanotechnology has enabled the development of functional nanomaterials with tailored surface, electronic, and magnetic properties, offering new opportunities for advanced and sustainable water treatment.

Spinel ferrites, particularly manganese ferrite ($MnFe_2O_4$), have attracted considerable attention because of their high chemical stability and strong magnetic response [10,11]. $MnFe_2O_4$ also exhibits a relatively narrow band gap (~2 eV), enabling visible-light activation. In addition, the mixed Mn–Fe redox system facilitated efficient electron transfer and reactive oxygen species generation, which are beneficial for photocatalytic degradation [12-14]. In addition, their magnetic properties enable facile recovery and reuse, addressing a key limitation of many nanoscale photocatalysts. However, the tendency of $MnFe_2O_4$ nanoparticles to agglomerate can significantly reduce their active surface area and catalytic efficiency, limiting their performance [15]. This challenge has motivated the development of composite systems to improve dispersion, stability, and charge separation.

Activated carbon is one of the most widely used carbon-based materials derived from biomass wastes, making it both sustainable and economically attractive. Their high surface area, well-developed porosity, and abundant surface functional groups enable strong interactions with organic pollutants through electrostatic attraction and hydrogen bonding [16-18]. Despite its excellent adsorption capacity, activated carbon also faces challenges related to its regeneration efficiency and energy-intensive production [19]. To overcome these limitations, increasing attention has been directed towards integrating activated carbon with metal oxides to form hybrid materials that combine adsorption and catalytic functionalities.

Therefore, $MnFe_2O_4$/activated carbon composites have emerged as the promising candidates for wastewater remediation. The incorporation of activated carbon has suppressed the nanoparticle agglomeration, enhances electron transfer, and improved structural stability, while $MnFe_2O_4$ contributed to photocatalytic and oxidative activity [20,21]. These synergistic effects have enabled the effective removal of diverse pollutants, including dyes, antibiotics, pesticides, and other complex organic compounds [22,23]. Beyond environmental remediation, such composites have also demonstrated potential in energy-related applications, such as electrocatalysis, further underscoring their multifunctional nature.

Despite growing interest, studies on $MnFe_2O_4$/activated carbon composites remain fragmented and largely pollutant-specific. Existing review articles have independently addressed ferrite-based photocatalysts, carbon-based adsorbents, and magnetic carbon composites [23-26]. However, a focused, integrated review dedicated to $MnFe_2O_4$/activated carbon composites encompassing synthesis strategies, physicochemical characterization, synergistic mechanisms, and multifunctional applications is lacking. This review fills this gap by systematically consolidating recent advances, critically evaluating synthesis strategies, physicochemical properties, and performance, and identifying future research directions for environmental remediation and sustainable energy applications

Manganese ferrite ($MnFe_2O_4$)

Synthesis and characteristics of $MnFe_2O_4$

Manganese ferrite ($MnFe_2O_4$) belongs to the family of spinel ferrites, which adopt a face- centered cubic (FCC) crystal structure where metal cations are distributed between tetrahedral (A) and octahedral (B) interstitial sites. The general formula of spinel ferrites is MFe_2O_4, with divalent cations (M^{2+} = Mn^{2+}, Co^{2+}, Ni^{2+}, Zn^{2+}, etc.) that typically occupying the A-sites, whereas Fe^{3+} and the remaining divalent cations occupy the B-sites. Depending on the cation distribution, the structure can be classified as a normal, inverse, or mixed spinel, and this arrangement strongly governs the magnetic, electronic, and catalytic properties. In particular, $MnFe_2O_4$ exhibits a relatively narrow band gap (~ 2 eV), high chemical and thermal stability, and superparamagnetic behavior at the nanoscale, making it as attractive for environmental and energy-related applications. A schematic illustration of the spinel lattice is presented in **Figure 1**, highlighting the distribution of divalent (M^{2+}) and trivalent (M^{3+}) cations between the tetrahedral (A) and octahedral (B) interstitial sites [27].

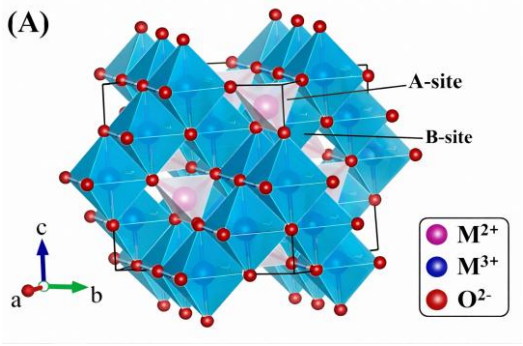

Figure 1 Schematic of the spinel ferrite structure, showing divalent (M^{2+}, purple) and trivalent (M^{3+}, blue) cations distributed between tetrahedral (A) and octahedral (B) sites, with oxygen anions (O^{2-}, red) completing the lattice [27].

X-ray diffraction (XRD) typically confirmed the crystalline nature of $MnFe_2O_4$. As shown in **Figure 2**, the XRD patterns reported in the literature have exhibited characteristic diffraction peaks at 2 θ = 18°, 30°, 35°, 43°, 53°, 57°, and 63°, corresponding to the (111), (220), (311), (400), (422), (511), and (440) planes of the cubic spinel structure (Fd − 3m). The absence of secondary phases indicated high purity. Williamson-Hall analysis in previous studies provided quantitative insights into crystallite size and lattice strain, revealing crystallite sizes in the nanometer range (e.g., ~9 - 10 nm) with measurable microstrain. These microstructural parameters are strongly influenced by the synthesis route: Sol-gel and co-precipitation methods, which promote rapid nucleation, typically yield smaller crystallite sizes and higher lattice strain, whereas hydrothermal and solvothermal routes enhance crystallinity, resulting in larger crystallite sizes and reduced strain due to prolonged crystal growth. Such variations directly affect surface reactivity and catalytic performance [28]. Magnetic hysteresis measurements further demonstrated the ferrimagnetic and soft magnetic nature of $MnFe_2O_4$, enabling rapid magnetic recovery from aqueous systems. Optical analysis has confirmed its narrow band gap (~ 2 eV), which supports visible- light photocatalysis.

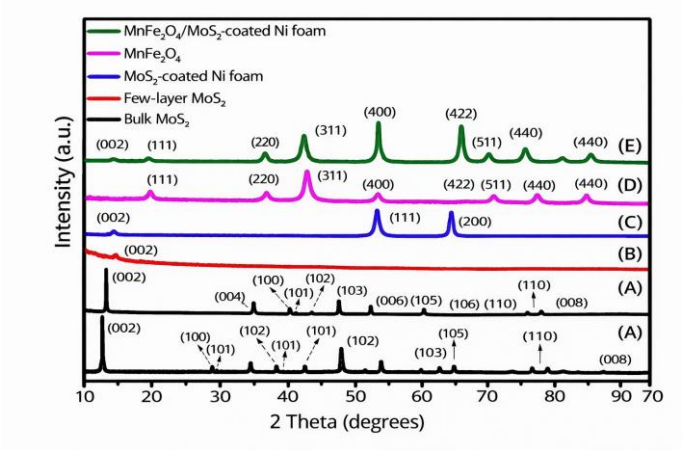

Figure 2 Representative XRD patterns of $MnFe_2O_4$-based materials reported in the literature, showing the characteristic diffraction peaks of the cubic spinel structure (space group Fd – 3m) [28].

Compared with other ferrites, $MnFe_2O_4$ exhibits superior magnetic susceptibility, facilitating recyclability through external magnetic separation. Its high dielectric response, oxidation resistance, and robust structural stability have expanded its applications beyond catalysis, including microwave absorption, drug delivery, MRI contrast enhancement, and energy storage technologies [29]. These combined advantages of tunable magnetic properties, structural stability, and sustainable recyclability underscore the potential of

$MnFe_2O_4$ as a functional nanomaterial across environmental and technological domains.

Among the various synthesis methods, the hydrothermal route has proven particularly effective, yielding uniform nanoparticles smaller than 20 nm with high reproducibility and cost efficiency. Morphological variations flakes, regular octahedra, and icosahedra significantly influence the oxygen vacancy densities, which in turn govern the catalytic activity and stability. Notably, icosahedral $MnFe_2O_4$ nanoparticles with minimal oxygen vacancies showed superior functionalization with myricetin, resulting in a 4.5-fold enhancement in size stability over 112 days [30].

Another key parameter is the cation inversion factor (λ), which describes the distribution of Mn^{2+} and Fe^{3+} between tetrahedral and octahedral sites. $MnFe_2O_4$ typically exhibits normal or partially inverse spinel configurations, with ferrimagnetic coupling between the sublattices. Although the effect of λ on magnetism is less pronounced than in other ferrites due to the $3d^5$ high-spin states of Mn^{2+} and Fe^{3+}, theoretical and experimental studies confirm that tuning λ alters the saturation magnetization ranging from ~5 μB (normal spinel) to ~3 μB (inverse spinel) [31]. Bulk $MnFe_2O_4$ demonstrates saturation magnetization of 3.3 - 4.5 μB per formula unit, higher than $NiFe_2O_4$ and $MgFe_2O_4$ and comparable to Fe_3O_4 and $CoFe_2O_4$. Additionally, nanoparticle size effects can shift λ, providing further control over the physicochemical performance.

Multiple synthesis routes have been reported for $MnFe_2O_4$, each influencing particle size, morphology, crystallinity, and ultimate performance in environmental and energy applications. Table 1 provides a comparative overview of the main synthetic approaches from the 6 cited references, highlighting their key features, advantages, limitations, and outcomes.

Table 1 Comparison of synthesis methods for $MnFe_2O_4$-based composites.

Method	Key Features / Conditions	Advantages	Limitations	Representative Results
Co-precipitation	$MnCl_2·4H_2O$, $FeCl_2·4H_2O$/$FeCl_3·6H_2O$; base NH_4OH; ~80 °C; pH adjusted until precipitation	Simple, low-cost, scalable; nanoparticles ~ 30 -50 nm; > 99% Cu^{2+} removal at pH 7	Particle size/purity sensitive to pH and base addition; prone to agglomeration without carbon support	Adsorption capacity ~ 199 mg g^{-1} for Cu^{2+}; particle size 30 - 50 nm [32]
Hydrothermal	$MnCl_2$/$FeCl_3$ + NaOH; autoclave 180 °C, 10 h; 1-step composite with sludge biochar	Simultaneous hydrothermal carbonization and $MnFe_2O_4$ nucleation; prevents agglomeration; enhanced surface area and magnetism	Requires autoclave (high pressure) and long reaction time	Pb^{2+} adsorption capacity 174.2 mg g^{-1}; Langmuir isotherm fit [33]
Sol-gel (with pyrolysis)	$MnSO_4·H_2O$ + $FeCl_3$ + citric acid; gel formation followed by pyrolysis at 500 - 700 °C; biochar from sawdust as support	Homogeneous dispersion of $MnFe_2O_4$ on biochar; enriched porosity and surface functionality; higher performance than commercial activated carbon	Requires medium-to-high temperature pyrolysis; outcome depends on composition and temperature	DCF adsorption capacity 352.2 mg g^{-1} (~ 3.5×commercial AC) [34]
Solvothermal (reflux)	$Fe(acac)_3$ & $Mn(acac)_2$ precursors; benzyl ether solvent (~ 300 °C) with oleylamine/oleic acid surfactants; 1 h reflux	Narrow size distribution, monodisperse nanocrystals (~ 9 nm); superparamagnetic (Ms ~ 56.4 emu g^{-1}); strong photocatalytic activity	Use of high-boiling solvents and organic surfactants; high reaction temperature	RhB degradation 96% within 6 h under UV [35]
Green synthesis	Plant extract (Azadirachta indica) as reducing/stabilizing agent; FCC crystal structure ($Fd\bar{3}m$)	Eco-friendly, low-energy, renewable; superparamagnetic properties; antibacterial activity	Variable extract composition affects reproducibility and particle size control	Average size ~ 59 nm; confirmed superparamagnetism [36,37]

As summarized in **Table 1**, each synthesis method imparts distinct physicochemical properties to $MnFe_2O_4$, with direct consequences for its catalytic and adsorptive behaviors. Co-precipitation is the most common method because of its simplicity, scalability, and low cost; however, the resulting particles are highly sensitive to pH and base concentration, which requires carbon supports to prevent agglomeration [32]. In contrast, hydrothermal methods enable the one-pot synthesis of $MnFe_2O_4$ integrated with biochar, simultaneously preventing nanoparticle agglomeration and improving surface accessibility, albeit requiring specialized autoclave equipment and longer reaction times [33]. The sol-gel method, particularly when combined with pyrolysis, produces homogeneously dispersed $MnFe_2O_4$ within biochar frameworks, significantly suitable in the commercial activated carbon for pollutant adsorption, albeit at higher temperatures [34]. Solvothermal reflux routes have excellent control over the particle size and monodispersity, yielding highly active nanocrystals but requiring expensive solvents and high-temperature processing [35]. Finally, green synthesis using plant extracts represents a sustainable and low-energy approach, producing superparamagnetic nanoparticles with added antibacterial properties, although reproducibility remains challenging owing to the variability in natural precursors [36,37].

Advantages and disadvantages of $MnFe_2O_4$ nanomaterials

The physicochemical features of manganese ferrite ($MnFe_2O_4$) provide a range of practical benefits for catalytic and adsorption processes. Its relatively narrow band gap allows excitation under visible light, offering an advantage over wide-band-gap semiconductors such as TiO_2 or ZnO which typically require UV irradiation. Upon illumination, $MnFe_2O_4$ can generate reactive oxygen species (ROS), that promote the degradation of persistent pollutants including dyes, pesticides, and pharmaceuticals. Another important advantage is its ferrimagnetic nature, which enables direct recovery from aqueous media using an external magnetic field. This recyclability not only reduces secondary waste but also represents a major improvement compared with conventional adsorbents that are difficult to separate after use. In addition, $MnFe_2O_4$ displays chemical and thermal stability, biocompatibility, and relatively low toxicity, which further broaden its potential for environmental and biomedical applications [38,39].

Experimental reports have confirmed these intrinsic strengths and reveal the influence of morphology and synthesis conditions to tailor the performance. For example, the solvothermal preparation of $MnFe_2O_4$ yielded cubic, flake, and capsule morphologies with distinct advantages: cubes exhibited superior electrical conductivity, capsule-like particles achieved the highest magnetic saturation, and flakes delivered remarkable photocatalytic activity, removing up to 98% of methylene blue with excellent reusability [40]. Similarly, solvothermally synthesized myrica rubra-like $MnFe_2O_4$ microspheres demonstrated exceptional microwave-assisted reduction of Cr(VI), achieving 96% removal within ten minutes under optimized acidic conditions substantially as commercial catalysts [41]. Beyond these applications, theoretical analyses emphasize multi-orbital hybridization in Mn–O and Fe–O bonds, which has exhibited its ferrimagnetic semiconductor behavior and unique optical properties, making the material attractive for optoelectronic and spintronic devices [42].

Nevertheless, several inherent drawbacks are limiting the widespread use of $MnFe_2O_4$. At the nanoscale, its high surface energy drives particle agglomeration, reducing the accessible surface area and thereby lowering the adsorption and catalytic efficiency [38]. The narrow band gap, which is beneficial for visible-light activation, also promotes the rapid recombination of photo-generated charge carriers, leading to diminished photocatalytic performance unless mitigated by coupling with conductive carbons, heteroatom doping, or heterojunction [42]. By controlling the reproducibility remains a challenge, as variations in pH, temperature and precursor ratios can result in size, morphology, and magnetic saturation [40]. Furthermore, although $MnFe_2O_4$ is magnetically recoverable, its different saturation magnetization can sometimes lower than that of other ferrites, reducing the separation efficiency in certain environmental and biomedical contexts. Surface modification or protective coatings are often required to enhance the stability and

dispersibility in aqueous and physiological systems [38].

Overall, $MnFe_2O_4$ has exhibited visible-light activity, magnetic recyclability, and structural stability, whereas morphology engineering further improves its performance. However, intrinsic challenges such as agglomeration, charge recombination, reproducibility, and scalability must be addressed. These limitations justify the growing emphasis on hybrid composites, particularly $MnFe_2O_4$ supported on activated carbon, which can stabilize nanoparticles, expand accessible surface area, and suppress charge recombination, thereby unlocking its full potential in environmental and technological applications.

Applications of $MnFe_2O_4$ (standalone)

Manganese ferrite ($MnFe_2O_4$) has been widely investigated as a promising material for environmental catalysis, particularly in pollutant degradation. Its Fenton-like catalytic activity facilitates the generation of reactive oxygen species (·OH and $\cdot O_2^-$) under broad pH conditions, which has promoted the efficient oxidation of dyes and refractory organics. For instance, halloysite-supported $MnFe_2O_4$ (HNT/$MnFe_2O_4$) has achieved over 90% removal of methylene blue at pH 4 - 10, showing superior hydrogen peroxide utilization efficiency and magnetic recoverability over multiple cycles [43]. Similarly, morphology-controlled $MnFe_2O_4$ nanostructures have demonstrated a high photocatalytic efficiency, with flake-shaped nanoparticles achieving nearly 98% degradation of methylene blue and retaining stability after repeated use [40]. These results have confirmed the potential of $MnFe_2O_4$ as an effective catalyst for wastewater purification, due to its visible-light activity, magnetic recyclability, and ability to operate under practical aqueous conditions.

In addition to water treatment, $MnFe_2O_4$ has also been employed in diverse technological domains. In gas sensing, pristine and Ni-doped $MnFe_2O_4$ nanoparticles prepared by co-precipitation method has exhibited efficient ammonia detection at room temperature, with 5 wt% Ni-doping enabling reliable sensing down to 200 ppm [44]. $MnFe_2O_4$ has further shown excellent electromagnetic wave absorption capabilities; when combined with conductive carbon nanotubes, $MnFe_2O_4$-based nanocomposites enhanced absorption coefficients by 2.5 - 3 times compared to pure ferrite across 5 - 20 GHz, making them as promising microwave absorbers [45]. In the energy sector, $MnFe_2O_4$ has been explored as an oxygen reduction reaction (ORR) electrocatalyst. Structural engineering via eutectic molten salt treatment has improved conductivity and increased the population of catalytically active Mn^{2+} sites, resulting in a positive 40 mV shift in the half-wave potential and a 2-fold enhancement in specific activity [46]. These findings highlight the multifunctional properties of $MnFe_2O_4$ in environmental remediation, sensing, microwave absorption, and energy conversion, thereby emphasizing its role as a sustainable spinel ferrite for next-generation technologies. A concise summary of these applications, including system modification and key performance metrics, is presented in **Table 2**.

Table 2 Selected applications of $MnFe_2O_4$ as a standalone material.

Application	System / Modification	Key Results	Ref.
Dye degradation (Fenton-like)	HNT/$MnFe_2O_4$	90% MB removal at pH 4 - 10; stable over 5 cycles; magnetic recovery	[43]
Photocatalysis	Flake $MnFe_2O_4$ morphology	98% MB degradation; high cycle stability	[40]
Gas sensor	Ni-doped $MnFe_2O_4$ (5 wt%)	Reliable NH_3 detection from 200 ppm at room temperature	[44]
Microwave absorption	$MnFe_2O_4$/CNT composites	2.5 - 3 ×higher EM absorption (5 - 20 GHz) vs. pure ferrite	[45]
ORR electrocatalysis (energy)	$MnFe_2O_4$ (EMS-treated)	+40 mV half-wave shift; ~ 2×higher mass/specific activity	[46]

Collectively, these applications demonstrate the potential of $MnFe_2O_4$ in environmental remediation, sensing, microwave absorption, and energy conversion applications. However, to overcome fundamental

challenges such as agglomeration, limited surface area, and charge recombination, recent efforts have increasingly focused on coupling $MnFe_2O_4$ with porous supports such as activated carbon. Such hybrid systems not only stabilize nanoparticles but also the expand surface accessibility and improve charge separation, thereby advancing the efficiency of pollutant removal and energy applications.

Activated carbon

Synthesis and characteristics of activated carbon

Activated carbon is a porous carbonaceous material that is widely regarded as one of the most effective adsorbents, primarily because of its exceptionally high surface area, hierarchical pore network, and rich surface chemistry. Activated carbon is predominantly derived from renewable biomass precursors, such as coconut shells, rice husks, durian shells, wood, and other agricultural by-products, as both cost-effective and sustainable for environmental and industrial use [47,48]. Depending on the processing method and intended use, activated carbon can be produced in several physical forms, including briquettes, granules, powders, and columnar shapes [49]. These morphologies strongly influence handling, surface accessibility, and adsorption kinetics, thereby determining their suitability in specific contexts such as adsorption, filtration, and catalysis.

A key feature of biomass-derived activated carbon is its exceptionally high surface area and a well-developed porosity [50]. The microporous network provides abundant adsorption sites for small molecules, whereas mesopores enhance diffusion pathways, making activated carbon as highly efficient for the removal of organic dyes, pesticides, heavy metals, and emerging contaminants from water and air [51]. Moreover, the surface chemistry of activated carbon is enriched with functional groups such as hydroxyl (–OH), carboxyl (–COOH), and amino ($–NH_2$) moieties, which play a pivotal role in adsorption through hydrogen bonding, electrostatic attraction, and π–π interactions [52]. These functionalities can be further tailored via chemical or physical activation for enhanced selectivity towards specific pollutants.

Recent studies have emphasized that the diversity of biomass precursors not only ensures sustainability but also provides a pathway for tuning the morphology and surface chemistry of activated carbon. For example, rice husk-derived activated carbon exhibits a higher silica content, whereas coconut shell-derived activated carbon provides superior hardness and mechanical strength, making it as suitable for industrial-scale adsorption and regeneration cycles [53]. Similarly, activated carbons prepared from unconventional feedstocks, such as durian shells or agricultural residues demonstrate surface areas and functional group densities, expanding their potential for low-cost adsorption and catalytic applications [50].

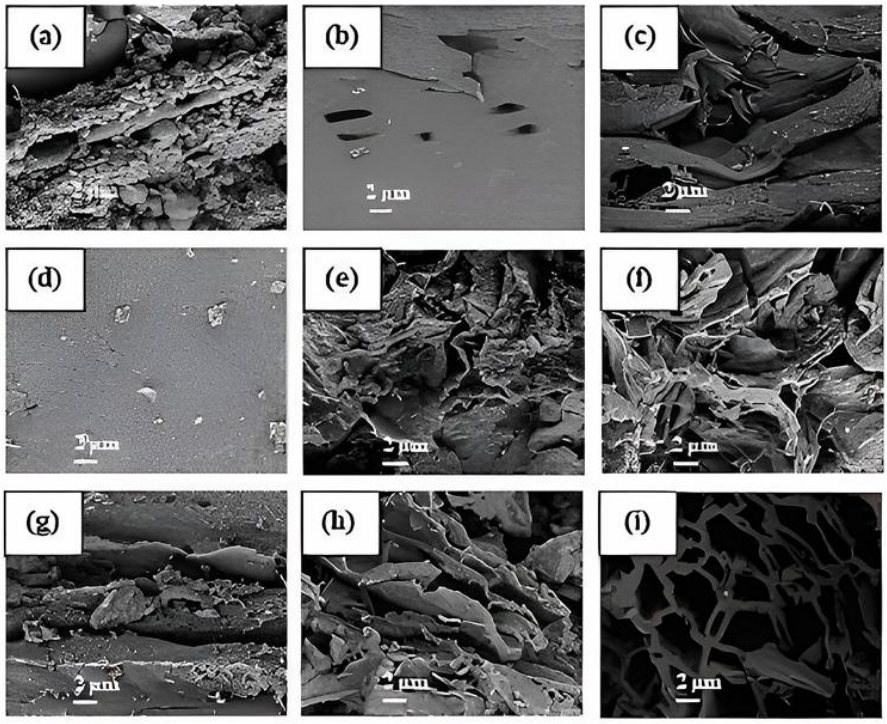

Figure 3 FESEM micrographs of biomass-derived activated carbons at an accelerating voltage of 5 kV, showing irregular fractured surfaces with interconnected pores that contribute to high surface area and adsorption capacity: (a) RSSAC, (b) RSSAC1/4, (c) RSSAC1/2, (d) DSAC, (e) DSAC1/4, (f) DSAC1/2, (g) PPAC, (h) PPAC1/4, and (i) PPAC1/2. RSSAC, DSAC, and PPAC represent activated carbons derived from rubber seed shell, durian shell, and palm petiole, respectively, while "1/4" and "1/2" denote KOH-to-biomass ratios of 1:4 and 1:2 [50].

Activated carbon is conventionally synthesized through physical or chemical activation. In physical activation, a carbonized precursor is exposed to oxidizing gases (steam or CO_2) at elevated temperatures, which progressively develops the pore structure. Chemical activation, in contrast, utilizes reagents such as KOH, $ZnCl_2$, or H_3PO_4 to simultaneously induce porosity and introduce functional groups that enhance adsorption affinity. Recently, increasing emphasis has been placed on activated carbon production from biomass waste, which not only reduces costs but also aligns with circular economic frameworks and sustainability objectives.

A wide spectrum of activation strategies was explored to optimize the yield, porosity, and surface chemistry. **Table 3** provides a comparative overview of the principal activation methods and highlights their operating conditions, advantages, limitations, and representative results [54-61].

Table 3 Comparison of synthesis methods for activated carbon.

Activation method	Activated carbon precursor (raw material)	Key features / conditions	Effect on carbon properties	Advantages	Limitations	Representative results & performance relevance
Physical Activation	Coal, lignite, wood char	Pyrolysis followed by steam or CO_2 activation (700 - 1,000 °C)	Moderate surface area, well-developed macropores and mesopores	No chemical additives, environmentally benign, scalable	High energy demand, lower surface area vs chemical activation	Coal-based AC showed enhanced pore development and improved CO_2 uptake, suitable for gas adsorption and diffusion-controlled catalysis [55]
Chemical Activation (KOH)	Corn stigmata, biomass residues	KOH impregnation and	Very high SBET, dominant	Extremely high surface area, excellent	Corrosive reagents,	KOH-activated corn stigmata exhibited wide pore size distribution and

Activation method	Activated carbon precursor (raw material)	Key features / conditions	Effect on carbon properties	Advantages	Limitations	Representative results & performance relevance
		carbonization (400 - 900 °C)	microporosity, abundant defects	adsorption capacity	wastewater treatment required	high adsorption capacity for organic pollutants, beneficial for adsorption–AOP systems [56]
Chemical Activation ($ZnCl_2$)	Coal slime, lignocellulosic waste	$ZnCl_2$ impregnation and activation (400 - 800 °C)	High micropore volume, uniform pore structure	Rapid activation, high surface area	Toxic Zn residues, limited environmental compatibility	$ZnCl_2$-activated coal slime achieved SBET of 918 m^2/g and strong dye and iodine adsorption, favoring fast adsorption kinetics [57]
Chemical Activation (H_3PO_4)	Durian shell, palm shell, coconut shell	Acid impregnation and carbonization (400 - 800 °C)	Mixed micro–mesoporous structure, oxygen-containing functional groups	High carbon yield, improved surface functionality	Acid handling, possible phosphate residues	Biomass-derived AC reached surface areas up to 2806 m^2/g, enhancing adsorption via pore filling and surface interactions, ideal as catalyst support [54]
Combined / Two-step Activation	Flax fiber, agricultural biomass	Pyrolysis followed by alkali impregnation (KOH, K_2CO_3) and high-T activation	Tunable micro/mesopore ratio, interconnected pore networks	Precise pore control, improved mass transport	Higher cost, process complexity	Flax fiber-derived AC showed enhanced porosity and electrochemical performance, relevant for catalytic and energy-related applications [58]

As indicated in **Table 3**, the activation pathways for activated carbon differ considerably in terms of efficiency, scalability, and environmental trade-offs. The choice of the activation route exhibits both performance and scalability. Physical activation offers chemical-free processing and environmental benignity, although it requires a high energy input and typically produces lower yields. Recent advances such as fast pyrolysis combined with physical activation have improved pore architecture and CO_2 uptake capacity [55]. Chemical activation is more versatile: KOH yields extremely high surface areas but generates corrosive waste streams [56], and $ZnCl_2$ provides rapid micropore formation yet increased the concerns regarding toxicity and residue management [57]. In contrast**,** while H_3PO_4 produces mesoporous carbons with high carbon yields and easier post-treatment, proving effective for both adsorption and energy storage [54]. More complex 2-step activation methods allow fine-tuning of the micro and mesoporosity, particularly advantageous when fibrous precursors are employed [58].

Recent developments have also emphasized the importance of predictive modeling and the role of machine learning in activated carbon production. Zou *et al.* [59] demonstrated that machine learning techniques can effectively forecast surface area, pore volume, and yield, highlighting the importance of process variables such as soaking and activation temperature. Furthermore, low-cost agricultural residues, such as arhar stalks was successfully transformed into porous activated carbon, proving the feasibility of scalable and eco-friendly precursors [60]. Studies on lacquer wood precursors have also revealed the promising outcomes for supercapacitor applications, thereby expanding the production of biomass-derived activated carbon [61]. These insights, together with advances in physical activation methods [55], indicate a trend towards integrating experimental, computational, and sustainability-oriented approaches into activated carbon research.

Henceforth, these studies underscore the dynamic progress in activated carbon production methods and highlight a clear view towards the utilization of renewable and waste biomass as precursors. By combining cost effective feedstocks with tailored activation strategies, current research not only advances material performance but also strengthens the integration of activated carbon production into sustainable and circular resource management frameworks.

Despite the advantages of advanced synthesis routes such as solvothermal and hydrothermal methods - which produce $MnFe_2O_4$/activated carbon composites with well-controlled morphology and enhanced performance - these approaches often involve higher energy consumption, longer reaction times, and limited scalability. In contrast, co-precipitation and related wet-chemical methods offer lower cost and easier scale-up but typically result in broader particle size distributions and reduced control over interfacial structure. These trade-offs highlight that superior laboratory-scale performance does not always translate to practical applicability; thus, synthesis route selection should balance performance requirements with economic and operational feasibility for the targeted application.

Advantages and disadvantages of activated carbon

Activated carbon exhibits several notable strengths, which make it as highly attractive for large-scale applications. Its immense surface area and tunable pore distribution enable the efficient adsorption of a wide variety of pollutants, including synthetic dyes, pesticides, antibiotics, and heavy metals [62,63]. The adsorption performance was further enhanced by the presence of surface functional groups (e.g., –OH, –COOH and $–NH_2$), which promote hydrogen bonding, electrostatic interactions, and π–π stacking with contaminants [70]. Another major advantage is the low cost and wide availability of biomass precursors such as coconut shells, rice husks, and other agricultural byproducts, particularly in regions with abundant waste resources [65]. These properties make activated carbon as a sustainable material for diverse environmental and industrial applications [63].

Despite these advantages, activated carbon has important limitations. In aqueous systems, powdered activated carbon is often difficult to separate and recover, requiring additional treatment steps that may generate secondary waste [64]. Regeneration of the activated carbon via thermal or chemical methods can be energy-intensive and sometimes incomplete, leading to a gradual loss of adsorption capacity and reduced cost-effectiveness over repeated cycles [62]. Moreover, large-scale production is frequently constrained by the high energy demand of the activation processes, especially those operating at elevated temperatures or using corrosive activating agents such as KOH or $ZnCl_2$ [66]. These drawbacks underscore the importance of ongoing research into alternative regeneration strategies, and the utilization of waste-derived precursors to enhance both the sustainability and economic viability of activated carbon.

Applications of activated carbon (standalone)

Activated carbon derived from various biomass and waste precursors has been extensively studied for pollutant removal applications. One of the most common uses is the adsorption of organic dyes, pesticides, and antibiotics. Activated carbon exhibits high efficiency owing to its large surface area, tunable pore structure, and abundance of surface functional groups. Factors such as precursor type, activation method, and surface modification significantly influences the adsorption performance, enabling activated carbon to effectively capture diverse organic molecules through electrostatic interactions, hydrogen bonding, and π–π stacking [67]. Recent advances in modification techniques have further enhanced the adsorption of recalcitrant contaminants, such as antibiotics and pesticides, highlighting the activated carbon as a sustainable adsorbent [68].

In addition to dye and antibiotic adsorption, activated carbon has found broad applications in water purification and industrial wastewater treatment. Biomass-derived activated carbon has demonstrated to efficiently remove heavy metals and other toxic pollutants from aqueous environments, while offering advantages such as cost-effectiveness and renewability [69,70]. For example, its high sorption capacity and reusability make it as particularly suitable for large-scale wastewater treatment, in which operational stability and selectivity are critical [71]. The continuous development in activated carbon synthesis and modification strategies have also expanded their applicability in advanced wastewater remediation processes.

In addition to conventional water treatment, activated carbon was applied in various niche industrial sectors. In the pharmaceutical field, activated carbon is widely recognized as a universal antidote because of its broad-spectrum adsorption capability, particularly against toxic organic compounds [72]. Moreover,

activated carbon -based systems have been explored for aquaculture, where phosphorus recovery from water using activated carbon composites not only reduces nutrient pollution, but also enables resource reuse [73]. These emerging applications demonstrate that activated carbon remains highly relevant not only in the traditional environmental purification but also for innovative resource management strategies across different industries. In practice, activated carbon is widely used in wastewater treatment for removing dyes, pesticides, antibiotics, and other pollutants, with its adsorption capacity proven efficient and adaptable across diverse water matrices. Beyond environmental remediation, it plays a key role in industrial wastewater purification, air and gas purification, and biomedical applications. These diverse uses underscore activated carbon as an indispensable material. **Table 4** highlights representative studies on its performance across broad applications. As shown, adsorption capacities vary with precursor type, surface chemistry, and modification method but consistently demonstrate high efficiency and reusability in environmental and industrial contexts.

Table 4 Representative applications of standalone activated carbon in pollutant removal and industrial systems.

Application	System / Precursor / Modification	Key Results / Observations	Ref.
Dye / pesticide / antibiotic adsorption	Biomass waste-derived activated carbon [67]; Modified activated carbon for heavy metals [68]	Adsorption capacities up to 400 - 650 mg/g for dyes (e.g., methylene blue); > 90% removal of antibiotics and pesticides depending on precursor and modification	[67,68]
Industrial wastewater treatment	Activated carbon from agricultural residues [70]; Biomass-derived activated carbon [71]	Heavy metal adsorption capacities typically 50 - 250 mg/g (Pb^{2+}, Cd^{2+} and Cr^{6+}); > 95% removal efficiency; stable over multiple regeneration cycles	[70,71]
Pharmaceutical antidote	activated carbon (general application) [72]	Recognized as universal antidote; rapidly adsorbs toxic organics and alkaloids in gastrointestinal tract; high efficiency even at low doses	[72]
Aquaculture water treatment	Activated carbon -based CaO_2 nanocomposites [73]	Phosphate adsorption capacity ~ 150 mg/g; > 85% removal from aquaculture wastewater; potential for phosphorus recovery and reuse	[73]

Preparation of $MnFe_2O_4$/activated carbon composites

Various synthetic strategies have been employed to fabricate $MnFe_2O_4$/ activated carbon composites, each yielding distinct structural characteristics and performance outcomes. Hydrothermal methods are widely applied because they generate composites with high crystallinity, uniform particle distribution, and stable magnetic properties. For instance, Cao *et al.* [74] have reported that hydrothermally prepared $MnFe_2O_4$/ activated carbon exhibited a larger surface area than compared to pristine $MnFe_2O_4$ and achieved outstanding activity in peroxydisulfate (PDS) activation, leading to 97.3% removal of norfloxacin [74]. The main advantage of this method is its ability to suppress nanoparticle agglomeration, although the synthesis process is relatively more complex.

Another effective route is the solvothermal method, which can significantly enhance the adsorption performance. Wang *et al.* [75] synthesized $MnFe_2O_4$/ activated carbon in a 1:2 mass ratio using a one-pot solvothermal process. The resulting composite has achieved an exceptionally high acetochlor adsorption capacity of 226 mg/g for acetochlor through mechanisms involving pore filling, hydrogen bonding, and π–π interactions. This demonstrates that carefully tuned synthesis conditions can substantially improve the pesticide removal efficiency.

The co-precipitation method offers the advantages of simplicity and milder synthesis conditions. Sabaa *et al.* [76] applied this method to obtain $MnFe_2O_4$/

activated carbon, which was then tested as an electrocatalyst for the oxygen reduction reaction (ORR). Their findings revealed that $MnFe_2O_4$/ activated carbon has outperformed other ferrite-based composites such as $CuFe_2O_4$/ activated carbon and $NiFe_2O_4$/ activated carbon. However, this technique can sometimes lead to non-uniform particle sizes and a tendency toward agglomeration, making the optimization of synthesis parameters essential.

Recently, increasing attention has been directed toward the use of waste-derived activated carbon as a sustainable and cost-effective precursor. Nguyen *et al.* [77] prepared activated carbon from durian shells, which was subsequently combined with $MnFe_2O_4$. The resulting composite has exhibited a high surface area of 518.9 m^2/g and achieved > 90% removal of indole from aqueous solution. Similarly, Do *et al.* [78] utilized coffee husks to derive activated carbon and obtained $MnFe_2O_4$/ activated carbon with an ammonium adsorption capacity of 15.97 mg/g. Such approaches have highlighted the potential of agricultural by-products to serve as low-cost feedstock while aligning with sustainability goals.

Ashfaq *et al.* [79] further demonstrated that waste biomass can produce multifunctional composites. By employing coconut shell-derived carbon and a hydrothermal synthesis route, they fabricated $MnFe_2O_4$/ activated carbon with excellent microwave absorption performance, achieving a minimum reflection loss of –38.4 dB at 1.8 mm thickness. This indicates that $MnFe_2O_4$/ activated carbon composites may extend their utility beyond environmental remediation to fields such as energy conversion and electromagnetic shielding.

Overall, the choice of the synthesis method strongly dictates the morphology, surface area, and dispersion of $MnFe_2O_4$ nanoparticles on the activated carbon matrix. The mass ratio of $MnFe_2O_4$ to activated carbon is also critical; for example, a 1:2 ratio has been reported to be optimal for acetochlor adsorption [75]. Therefore, the combination of appropriate synthesis strategies with sustainable precursors is therefore key to increase the efficiency and applicability of these composites in both environmental and energy-related domains.

A comparative overview of reported synthesis strategies for $MnFe_2O_4$/activated carbon composites is presented in **Table 5**. This table outlines variations in activated carbon precursors, preparation methods, mass ratios, and corresponding performance metrics. Such an overview enables readers to clearly evaluate the influence of structural properties and functional efficiency of $MnFe_2O_4$/activated carbon composites across different synthesis approaches. As shown in **Table 5**, the preparation method and precursor type not only determine the physicochemical characteristics of $MnFe_2O_4$/activated carbon but also directly affect its adsorption and catalytic performance.

Table 5 Preparation of $MnFe_2O_4$/AC Composites and their targeted application.

No	Precursor		Method	Ratio ($MnFe_2O_4$: Activated Carbon)	Target Application/ Degradation	Ref
	$MnFe_2O_4$	Activated Carbon				
1	$MnCl_2.4H_2O$ + $FeCl_3.6H_2O$	Coffee Husk	Hydrothermal	1:3	Ammonium Removal From Wastewater	[78]
2	$Mn(NO_3)_2$ + $Fe(NO_3)_3.9H_2O$	Activated carbon + Peroxydisulfate	Hydrothermal	0.2:0.5 g	Norfloxacin (NOR) Degradation Via PDS Activation	[74]
3	$Mn(NO_3)_2$ + $Fe(NO_3)_3.9H_2O$	Carbon Vulcan XC – 72R	Co -Precipitaion	Not Mentioned	ORR Catalyst in MFCs (Electrocatalysis)	[76]
4	$MnCl_2.4H_2O$ + $Fe(NO_3)_3.9H_2O$	Durian Peel	Impregnation - Calcination	1.29 g Mn + 4.22 g Fe: 5 g AC	Indole (IDO) Removal	[77]
5	Fe^{3+} + Mn^{2+}	Coconut Shell	Onepot Solvothermal	1:2	Acetochlor removal & Degradation (PMS Oxidation)	[75]
6	$MnCl_2$ + $FeCl_3$	Coconut Shell	Hydrothermal Approach	1:1, 1:2, 1:3	Microwave Absorption (EM pollution control)	[79]

Structural characterization

Comprehensive structural characterization is essential to verify the successful synthesis of $MnFe_2O_4$/activated carbon composites and to establish correlations between their structural properties and functional performance. A combination of XRD, SEM/TEM, FTIR/XPS, BET, and VSM techniques was applied to confirm the phase formation, morphological features, surface functionalities, porosity, and magnetic behavior of the composites.

X-ray diffraction (XRD) has consistently confirmed the formation of the spinel $MnFe_2O_4$ phase, with sharp and well-defined diffraction peaks indicating high crystallinity. In several reports, the characteristic peaks of $MnFe_2O_4$ were detected alongside the broad amorphous peaks of carbon, confirming the successful integration of the 2 components. Moreover, the XRD patterns show reduced agglomeration when $MnFe_2O_4$ was supported on activated carbon compared with pristine ferrite, highlighting the stabilizing role of the carbon matrix [74,76].

Microscopic observations using SEM and TEM were validated further validation. SEM images typically showed that the raw activated carbon has exhibited large particles with irregular pores, whereas the $MnFe_2O_4$/activated carbon composites displayed nanoparticles uniformly distributed within the porous carbon framework [77,78]. TEM and high-resolution TEM studies also provided evidence of well-dispersed nanosized $MnFe_2O_4$ particles anchored onto the activated carbon, effectively preventing particle agglomeration [76]. Such morphological control is critical for increasing the available surface area and enhancing the accessibility of pollutants to active sites.

Spectroscopic analyses (FTIR and XPS) revealed the presence of functional groups such as –OH, C=O, and Fe–O, which contribute to adsorption and catalytic activity [74,78,79]. The FTIR spectra showed distinct bands assigned to Mn–O and Fe–O vibrations, confirming the successful incorporation of ferrite into the activated carbon support. Meanwhile, XPS analysis provided insight into the oxidation states of Mn and Fe, as well as the interaction between metal oxides and surface oxygen functionalities of activated carbon, which are vital for radical generation during advanced oxidation processes.

BET surface area analysis demonstrated that the incorporation of activated carbon has significantly enhanced the porosity compared to that of pristine $MnFe_2O_4$. For example, durian shell-derived activated carbon supported $MnFe_2O_4$ has achieved a high specific surface area of 518.9 m^2/g with a pore volume of 0.106 cm^3/g [83]. These properties are directly correlated with improved adsorption capacities, as the large surface area and hierarchical porosity facilitated pore filling, hydrogen bonding and π–π interactions with organic contaminants.

In addition to structural and surface characteristics, the magnetic behavior of $MnFe_2O_4$/activated carbon composites play a crucial role in their functional performance. Owing to the spinel ferrite structure of $MnFe_2O_4$, these composites typically exhibit ferrimagnetic or superparamagnetic behavior at the nanoscale, arising from antiparallel spin coupling between metal cations at tetrahedral (A) and octahedral (B) sites [80,81]. Activated carbon incorporation does not eliminate the intrinsic magnetism of $MnFe_2O_4$ but moderates particle agglomeration and preserves sufficient saturation magnetization for effective magnetic responsiveness.

This property enables rapid, efficient separation of the composite from aqueous media using an external magnetic field, which is highly advantageous for practical wastewater treatment [82]. Magnetic recovery simplifies post-treatment handling, reduces secondary sludge formation, and enhances recyclability over multiple adsorption/photocatalytic cycles [83]. Compared to non-magnetic carbon-based adsorbents, $MnFe_2O_4$/activated carbon composites offer superior operational sustainability and cost-effectiveness [84].

Beyond environmental remediation, the magnetic characteristics of $MnFe_2O_4$/activated carbon composites support energy-related applications. Magnetic ferrite domains facilitate electron transport and interfacial charge transfer, benefiting electrocatalytic reactions such as the oxygen reduction reaction (ORR) [85]. Furthermore, the synergy of magnetic loss from $MnFe_2O_4$ and dielectric loss from activated carbon enhances electromagnetic wave attenuation for microwave absorption and interference shielding [86].

Finally, magnetic measurements using VSM highlighted the importance of magnetic properties for

practical applications. The composites have exhibited strong magnetization, ensuring facile separation from the treated solutions after use [75,79]. This characteristic provides a distinct operational advantage, enabling easy recovery and reusability of the material without causing secondary pollution. These structural characterizations confirm that $MnFe_2O_4$/activated carbon composites have successfully integrated the physicochemical benefits of both components: the magnetic and redox activity of $MnFe_2O_4$ and the high surface area and functionalized porosity of the activated carbon. The synergy between these features underpins the superior adsorption and catalytic performance reported in subsequent application studies.

Adsorption and photocatalytic performance

The pollutant removal performance of $MnFe_2O_4$/activated carbon composites has been extensively investigated, and results highlighted their multifunctional properties. Depending on the synthesis route, precursor materials, and operating conditions, these composites demonstrate remarkable efficiency relative to pristine $MnFe_2O_4$ or activated carbon alone, although the reported performances vary significantly depending on the synthesis route and operational parameters. For pesticide removal, the solvothermally synthesized $MnFe_2O_4$/activated carbon with a 1:2 mass ratios have achieved an outstanding adsorption capacity of 226.76 mg g^{-1} for acetochlor under optimized laboratory conditions (25 °C, adsorbent dosage 0.2 g L^{-1}, and single-solute system) [75]. The removal process was attributed to multiple mechanisms, including pore filling, hydrogen bonding, and π–π interactions between the aromatic rings of acetochlor and the carbon surface. Importantly, regeneration tests have confirmed that the material retained more than 90% degradation efficiency after PMS activation, although its adsorption capacity gets decreased by approximately 50% after repeated cycles [75].

For antibiotic degradation, a hydrothermally synthesized composite was shown to effectively activate peroxydisulfate (PDS) for norfloxacin removal. The system achieved 97.33% degradation under optimized conditions (0.15 A current, 0.100 g L^{-1} catalyst, 10 mmol L^{-1} PDS, and 5 mg L^{-1} NOR), which represents idealized laboratory settings rather than realistic wastewater conditions [74]. This result highlights the strong potential of $MnFe_2O_4$/activated carbon composites in advanced oxidation processes of pharmaceutical pollutants. Studies have also demonstrated promising results for nutrient removal, particularly ammonium. A composite prepared from coffee husk-derived AC (ratio 1: 3) has exhibited an adsorption capacity of 15.97 mg/g at pH 7 and an equilibrium time of 80 min [78]. The high performance was attributed to the abundant oxygen-containing functional groups on the AC surface, which enhanced the electrostatic attraction and ion exchange with ammonium ions.

$MnFe_2O_4$/activated carbon composites have also depicted a high efficiency in removing organic contaminants. A composite derived from durian shell AC has exhibited excellent performance. Response surface methodology (RSM) optimization has revealed > 90% removal at near-neutral pH (7.4) in a batch system with synthetic wastewater, indicating favorable adsorption performance under controlled conditions [77]. Thermodynamic analysis further confirmed the spontaneity of the adsorption ($\Delta G° < 0$).

In addition to the adsorption-driven removal, the superior photocatalytic performance of $MnFe_2O_4$/activated carbon composites were supported by experimental evidence reported in recent studies. Radical scavenging experiments employing isopropanol, benzoquinone, and ammonium oxalate demonstrated that hydroxyl radicals (•OH) and photogenerated holes (h^+) are the dominant reactive species responsible for pollutant degradation, whereas superoxide radicals ($•O_2^-$) play a secondary or condition-dependent role. Furthermore, electron spin resonance (ESR) measurements provide direct confirmation of •OH and $•O_2^-$ formation during visible-light irradiation or oxidant activation, indicating effective charge separation and sustained reactive oxygen species (ROS) generation in carbon-supported $MnFe_2O_4$ systems. These experimental findings corroborate that the enhanced photocatalytic performance of $MnFe_2O_4$/activated carbon composites, relative to bare $MnFe_2O_4$, originates from the improved electron transport through the conductive carbon matrix, suppressed electron–hole recombination, and efficient redox cycling of Fe^{2+}/Fe^{3+} and Mn^{2+}/Mn^{3+} species.

In addition to environmental applications, $MnFe_2O_4$/activated carbon composites have attracted

attention for electromagnetic absorption and energy conversion applications. Coconut shell–based composites synthesized via a hydrothermal approach has achieved a minimum reflection loss of –38.4 dB at 1.8 mm thickness, with an effective absorption bandwidth of 6.2 GHz in the Ku-band range [79]. Similarly, $MnFe_2O_4$/activated carbon demonstrated superior oxygen reduction reaction (ORR) activity compared to $NiFe_2O_4$/ activated carbon and $CuFe_2O_4$/activated carbon, with a more favorable onset potential and current density [76]. These results suggest that $MnFe_2O_4$/activated carbon is not limited to wastewater treatment but may also play a role in renewable energy and electromagnetic shielding applications.

Although $MnFe_2O_4$/activated carbon composites demonstrate the enhanced adsorption and photocatalytic performance compared to their individual components, direct comparison among reported studies remains challenging owing to substantial variations in the experimental conditions. Adsorption capacities are strongly influenced by parameters such as pH, initial pollutant concentration, contact time, and adsorbent dosage, whereas the photocatalytic efficiency depends on the light source, irradiation intensity, catalyst loading, and reaction duration. High removal efficiencies reported under optimized laboratory conditions such as acidic media, low contaminant concentrations, or high light intensity may therefore overestimate the performance under realistic operational environments. These factors highlight the importance of evaluating $MnFe_2O_4$/activated carbon composites in terms of removal efficiency operational feasibility, durability, and scalability.

To improve the comparability of the reported performance data, the adsorption and photocatalytic results discussed in this review were interpreted within a common experimental context. Adsorption performance is primarily compared using capacity values normalized per unit mass of adsorbent (mg g^{-1}), while considering key operating parameters such as solution pH, initial pollutant concentration, and contact time. Similarly, photocatalytic activity is contextualized based on the degradation efficiency and reaction time under comparable light sources (UV or visible) and catalyst loadings. This contextualization allows for a more balanced assessment of reported results while avoiding the over interpretation of isolated high-performance values.

Mechanism of adsorption and degradation

The adsorption and degradation efficiencies of $MnFe_2O_4$/activated carbon composites can be attributed to a combination of physicochemical properties, including porosity, surface functionalities, and the redox activity of the ferrite phase. Several complementary mechanisms have been proposed to explain this performance. The overall synergistic adsorption-degradation mechanism is illustrated in **Figure 4**, demonstrating the complementary roles of activated carbon in adsorption and $MnFe_2O_4$ in reactive oxygen species generation and catalytic degradation.

The adsorption processes are primarily governed by both physical and chemical interactions. Pore filling is the dominant pathway, as the hierarchical porosity of activated carbon provides abundant adsorption sites for organic molecules and ions. Hydrogen bonding between the surface hydroxyl or carboxyl groups and pollutant molecules further enhances affinity [77,78]. In addition, π–π and n–π interactions are frequently reported, particularly in the removal of aromatic pollutants such as acetochlor and indole, where the π-electron systems of the contaminants interact with the aromatic domains of the activated carbon [75,77]. Thermodynamic analyses, including negative ΔG° values have confirmed the spontaneity of these adsorption processes, suggesting that both physisorption and chemisorption occur simultaneously [77].

In photocatalytic and advanced oxidation processes (AOPs), $MnFe_2O_4$ provides redox-active sites that facilitate electron transfer, whereas activated carbon suppresses electron–hole recombination and promotes radical generation. Upon activation (e.g., peroxydisulfate or peroxymonosulfate), reactive oxygen species such as hydroxyl radicals (•OH) and sulfate radicals ($SO_4^{\bullet-}$) are generated [74,75]. These highly reactive species are capable of oxidizing recalcitrant pollutants such as norfloxacin, leading to near-complete degradation under optimized conditions. The synergistic role of activated carbon is particularly critical: by enhancing electron mobility and providing conductive networks, activated carbon not only increases catalytic activity, but also ensures that a larger number of active sites are accessible to pollutants.

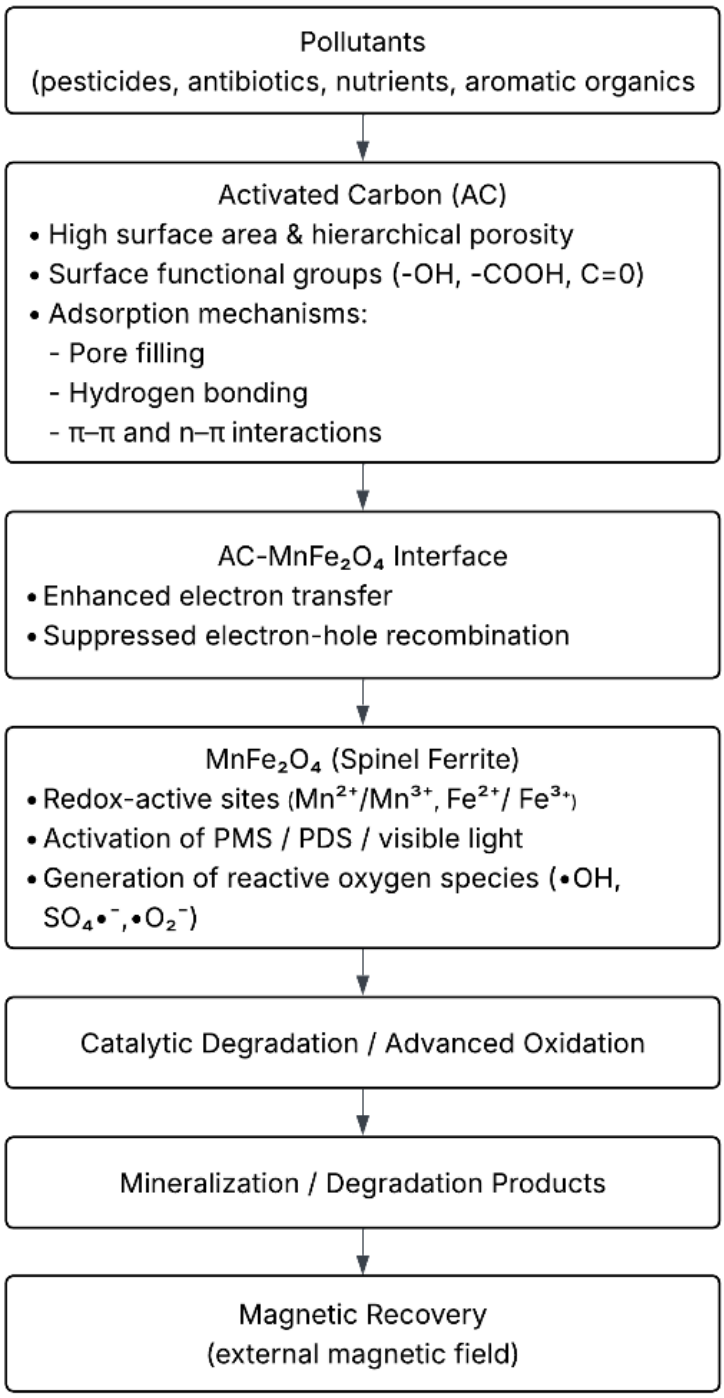

Figure 4 Conceptual schematic of the synergistic adsorption-degradation mechanism of $MnFe_2O_4$/activated carbon composites.

Compared to bare $MnFe_2O_4$, incorporation of activated carbon significantly enhances interfacial electron transport and charge separation due to its high electrical conductivity and efficient electron-mediating pathways [87]. Carbonaceous substrates like biochar or activated carbon act as electron shuttles between $MnFe_2O_4$ active sites and oxidants, altering selectivity, improving electron transfer in advanced oxidation processes (AOPs), and directly participating in charge carrier dynamics and catalysis.

This role in promoting electron mobility and suppressing electron–hole recombination is observed in related metal–carbon composites, where the conductive carbon network lowers charge-transfer resistance and

prolongs charge carrier lifetimes, yielding higher photocatalytic degradation efficiencies than pristine metal oxides [88].

From a charge-transfer perspective, the $MnFe_2O_4$/activated carbon interface establishes an efficient electron migration pathway. Upon light irradiation or oxidant activation, electrons generated at the $MnFe_2O_4$ surface rapidly transfer to the conductive carbon matrix, which serves as an electron acceptor and transport medium. This directional flow promotes charge carrier separation and delivers electrons to surface-active sites, effectively activating oxidants such as peroxymonosulfate (PMS) or peroxydisulfate (PDS) [89].

At the molecular level, enhanced photocatalytic and AOP performance stems from dual redox cycling between Fe and Mn species in the $MnFe_2O_4$ lattice, governing oxidant activation and sustained reactive oxygen species (ROS) generation [90]. In heterogeneous Fenton-like reactions with H_2O_2, the Fe^{2+}/Fe^{3+} couple primarily generates hydroxyl radicals (–OH), with Fe^{2+} reducing H_2O_2 to –OH and Fe^{3+}, requiring continuous regeneration of Fe^{2+} [91]. The Mn^{2+}/Mn^{3+} pair accelerates Fe^{3+} reduction to Fe^{2+}, boosting redox efficiency and ROS production

The magnetic properties of $MnFe_2O_4$ have provided a further operational advantage by allowing composites to be easily recovered from the treated solutions using an external magnetic field [79]. This has facilitated the reusability and minimizes the risk of secondary pollution. Indeed, regeneration studies show that $MnFe_2O_4$/ activated carbon can maintain over 90% degradation efficiency after multiple cycles, although adsorption capacities may gradually decline due to surface fouling or partial deactivation of active sites [74][75]. Heat-assisted activation of PMS was reported as an effective method for restoring catalytic activity, offering practical pathways for long-term applications [75].

particularly in carbon-supported composites that facilitate electron transfer (e.g., $MnFe_2O_4$@honey locust carbon) [92].

In addition to redox-active metal centers, oxygen vacancies on the $MnFe_2O_4$ surface play a pivotal role in regulating catalytic activity. These defect sites function as electron-trapping centers and as preferential adsorption sites for oxidants and dissolved oxygen, thereby lowering the activation energy for electron transfer. Oxygen vacancies also facilitate the interconversion between Fe^{2+}/Fe^{3+} and Mn^{2+}/Mn^{3+} species, enhancing redox cycling efficiency and sustaining reactive oxygen species generation during photocatalytic and AOP processes [93,94].

In PMS activation, surface Mn^{2+} directly produces SO_4- $^{-}$, while Mn^{3+} regenerates Fe^{2+} from Fe^{3+}, increasing radical diversity and ROS density versus single-metal catalysts. Studies on $MnFe_2O_4$-modified biochar confirm –OH and SO_4- –as dominant species in PDS activation, with exposed Fe/Mn sites improving electron transfer and ROS yields [95-97]. This is corroborated in H_2O_2 systems, where $MnFe_2O_4$ nanocomposites (e.g., $MnFe_2O_4$@MoS_2) enhance ROS (–OH, $–O_2^-$ and $^1O_2$) via Fe/Mn redox cycling and oxygen vacancies [98]

Overall, the mechanisms underlying $MnFe_2O_4$/ activated carbon performance arise from a synergistic combination: the magnetic and redox properties of $MnFe_2O_4$, the high porosity and functional groups of activated carbon, and the effective suppression of charge recombination in catalytic processes. This synergy shows that $MnFe_2O_4$/ activated carbon consistently outperforms, making it as a versatile and highly efficient material for pollutant removal and related applications.

Table 6 provides a consolidated overview of structural characterizations, adsorption performance, and mechanistic insights, highlighting key findings and serving as a reference for evaluating the potential of $MnFe_2O_4$/activated carbon composites in environmental and energy applications.

Table 6 Structural characterizations, adsorption performances, and mechanistic insights of $MnFe_2O_4$/activated carbon composites.

Ref	Sample / Ratio	Characterization	Main Results
[78]	$MnFe_2O_4$/ activated carbon (Coffee Husk activated carbon, 1:3)	SEM, FTIR, Adsorption (batch)	SEM: Activated carbon → large particles with few pores; $MnFe_2O_4$/ activated carbon → uniformly dispersed small

Ref	Sample / Ratio	Characterization	Main Results
			particles. FTIR: –OH, C–O, Fe–O groups. Adsorption: NH_4^+ capacity 15.97 mg/g at pH 7 (80 min, 1.5 g/L).
[74]	$MnFe_2O_4$/ activated carbon	SEM-EDS, XRD, FTIR, XPS, Adsorption/Degradation NOR	SEM/XRD: Spinel structure with reduced agglomeration. FTIR/XPS: –OH, C=O, Fe–O groups. NOR degradation: 97.33% (optimum: 0.15 A, 0.100 g/L catalyst, 10 mmol/L PDS, 5 mg/L NOR). Stable, no secondary pollution.
[76]	$MnFe_2O_4$/ activated carbon vs (vs $NiFe_2O_4$/ activated carbon, $CuFe_2O_4$/ activated carbon)	XRD, Raman, FTIR, BJH, SEM, HR-TEM, ESR, CV, LSV	$MnFe_2O_4$/ activated carbon showed best ORR performance (Eonset −0.223 V, jK ≈ −5 mA/cm², Tafel slope 330 mV/dec). ESR: Highest ΔHpp correlating with ORR activity. Mechanism: $4e^-$ pathway (pH 7). Potential Pt alternative in MFCs.
[77]	$MnFe_2O_4$/ activated carbon (durian shell activated carbon)	SEM, BET, RSM optimization, Adsorption (isotherm/kinetic)	BET: Surface area 518.9 m²/g, pore volume 0.106 cm³/g. Indole removal: > 90% at pH 7.4. Kinetics: Elovich & Temkin ($R^2 \geq 0.99$). Thermodynamics: $\Delta G° < 0$ (spontaneous). Mechanisms: Pore filling, π–π, n–π, H-bonding. Reusable up to 3 cycles.
[75]	$MnFe_2O_4$/ activated carbon (1:2, coconut shell AC)	XRD, SEM, Adsorption & Regeneration	Acetochlor adsorption: Max 226.76 mg/g (25 °C, 0.2 g/L). Mechanisms: Pore filling, H-bonding, π–π. Regeneration with PMS (70 °C, ≥ 9.6 mM): > 90% degradation but ~ 50% drop in capacity. Stable, magnetic, easily separable.
[79]	$MnFe_2O_4$/ activated carbon (coconut shell activated carbon, ratios 1:1, 1:2, 1:3)	XRD, SEM, XPS, Microwave Adsorption	XRD/XPS: Cation disorder and defect structures enhanced ionic conductivity. SEM: Nano-domain ferrite. Microwave absorption: Optimum at 1:2 ratio, RLmin -38.4 dB (1.8 mm), EAB 6.2 GHz (11.8 - 18 GHz, Ku-band).

As shown in **Table 6**, $MnFe_2O_4$/ activated carbon composites demonstrated a synergistic enhancement of adsorption and catalytic functions, regardless of the pollutant type or synthesis approach. The comparative results highlight that while different precursors and preparation methods yield variations in performance, the integration of $MnFe_2O_4$ with activated carbon remains as a reliable strategy to improve the efficiency. These findings collectively reinforce the versatility of $MnFe_2O_4$/ activated carbon composites and provide a solid foundation for their constant development for practical applications.

Comparative adsorption and photodegradation mechanisms

For pristine $MnFe_2O_4$, the removal of pollutants primarily occurs through catalytic and oxidative pathways rather than via strong adsorption, owing to its relatively limited surface area and porosity. $MnFe_2O_4$ acts as a semiconductor catalyst in advanced oxidation processes (AOPs), where light or oxidant activation excites electrons and generates electron-hole pairs that facilitate redox reactions and reactive oxygen species (ROS) formation (e.g., •OH, $SO_4^{\bullet-}$). Redox cycling between Fe^{2+}/Fe^{3+} and Mn^{2+}/Mn^{3+} is common to these processes, enabling pollutant degradation via oxidative pathways, although rapid charge recombination can limit the performance of $MnFe_2O_4$ systems. This catalytic behavior has been documented as part of the broader environmental applications of $MnFe_2O_4$-based nanoparticles [99,100].

In contrast, activated carbon is a well-known adsorbent with high surface area and hierarchical porosity that facilitates pollutant uptake primarily through physical and chemical interactions such as pore filling, π–π interactions, and hydrogen bonding [101]. The strong adsorptive capacity of activated carbon allows it to concentrate target molecules at its surface; however, activated carbon lacks intrinsic photocatalytic activity and cannot generate ROS without a catalytic or

oxidant component. These adsorption mechanisms are well established for carbonaceous materials derived from various biomass feedstocks [102].

When $MnFe_2O_4$ doped with activated carbon, synergistic mechanisms emerge that combine adsorption and catalytic degradation: Activated carbon adsorbs and concentrates on the pollutants near the active sites of $MnFe_2O_4$, by enhancing local reactant availability, while its conductive carbon network improves electron transport and suppresses electron-hole recombination, leading to more efficient ROS generation under AOP conditions [103]. This synergistic behavior has been demonstrated in $MnFe_2O_4$/activated carbon composites used for peroxydisulfate activation, where quenching tests and spectroscopic analyses reveal that both free radicals (•OH, SO_4•$^-$ and •O_2^-) and non-radical pathways contribute to degradation, supported by enhanced charge transfer between $MnFe_2O_4$ and the carbon matrix [104]. $MnFe_2O_4$/activated carbon composites has demonstrated the individual components by leveraging adsorption-assisted catalysis, improved charge separation, and more sustained radical production, illustrating that the composite's mechanism is not a simple sum of its parts but a true integration of adsorption and photodegradation pathways.

Energy-related applications of $MnFe_2O_4$/ activated carbon composites

In addition to environmental remediation, $MnFe_2O_4$/activated carbon composites have gained increasing attention for energy-related applications, owing to their synergistic magnetic, electronic, and structural properties. The integration of spinel ferrite $MnFe_2O_4$ and conductive activated carbon creates a hybrid system with enhanced charge transport, abundant active sites, and tunable interfacial properties, which are essential for electrochemical and energy conversion applications. Furthermore, the redox ferrite nature of $MnFe_2O_4$ has been explored for energy conversion applications such as solar-driven CO_2 splitting, where redox cycling and energy integration are central to the process [105]. Additionally, conductive carbon matrices similar to activated carbon was observed to enhance electron transport and catalytic efficiency in ferrite/carbon hybrid systems, supporting the broader relevance of carbon-supported ferrites for energy conversion processes beyond environmental remediation [106].

From a practical perspective, production cost, energy consumption, and environmental risks must be considered. Although $MnFe_2O_4$/activated carbon composites often use low-cost biomass precursors for activated carbon, the overall energy demand remains significant due to high-temperature carbonization/activation and hydrothermal/solvothermal ferrite synthesis [107]. Optimizing synthesis toward lower temperatures, shorter times, and scalable one-pot methods is essential for economic viability. Additionally, potential release of nanoscale ferrite particles during long-term use or regeneration raises environmental and health concerns. While the magnetic properties of $MnFe_2O_4$ enable efficient recovery, further studies are needed to assess nanoparticle stability, metal leaching, and ecotoxicological effects under realistic conditions [108]. Addressing these challenges is crucial for translating laboratory success into safe, sustainable real-world applications.

Conclusion and future perspectives

$MnFe_2O_4$/activated carbon composites have emerged as highly promising multifunctional materials, integrating the magnetic/redox activity of manganese ferrite with the high surface area, porosity, and rich surface chemistry of activated carbon. Extensive studies confirm well-dispersed crystalline spinel $MnFe_2O_4$ within carbon matrices, yielding outstanding performance across diverse applications. These composites exhibit high adsorption capacities for pesticides, antibiotics, nutrients, and aromatic organics, alongside potential in microwave absorption, electrocatalysis, and energy conversion. Their superiority arises from synergy: $MnFe_2O_4$ provides redox-active sites and magnetic separability, while activated carbon facilitates electron transfer, suppresses charge recombination, and offers abundant functional groups for pollutant interactions. Composites also demonstrate good recyclability, minimal metal leaching, and stable magnetism over repeated cycles.

While most studies use synthetic wastewater in batch reactors, limited work on related systems shows promise in real matrices like tap/river water. However, comprehensive assessments in complex industrial

effluents or continuous-flow setups remain scarce, with challenges including competing ions, natural organic matter, fouling, residence time distribution, and regeneration. Despite advances, translating these materials to practical technologies requires addressing scalable/reproducible synthesis (especially from heterogeneous waste precursors), long-term stability, detailed mechanistic elucidation (e.g., ROS pathways, intermediates via *in situ* characterization/modeling), and operational constraints.

Future research should prioritize green, cost-effective, scalable synthesis from biomass/industrial wastes; pilot/field-scale trials for performance validation, safety, and toxicity assessment; and hybrid integrations (e.g., with membranes, electrochemistry, or solar photocatalysis) for enhanced robustness. Expanding to energy conversion, electromagnetic shielding, and smart materials will broaden impact.

In summary, $MnFe_2O_4$/activated carbon composites represent a transformative class at the nexus of environmental remediation, energy, and advanced technologies. Overcoming scalability, mechanistic, and implementation challenges positions them as platforms for sustainable solutions.

Acknowledgements

This review article was supported by the School of Chemical Sciences, Universiti Sains Malaysia, and the Department of Physics, Universitas Sumatera Utara.

Declaration of generative AI in scientific writing

This manuscript was prepared without the use of any generative AI tools. No content creation or data interpretation was performed using AI. All authors take full responsibility for the content and conclusion of this work.

CRediT author statement

Dinda Amilia: Conceptualization; Methodology; Investigation; Formal analysis; Writing - Original draft. **Noor Haida Mohd Kaus**: Funding acquisition; Supervision; Project administration; Writing - Original review & editing. **Muhammadin Hamid**: Writing - Original review & editing; Project administration; Supervision.

References

[1] SY Qattan. Harnessing bacterial consortia for effective bioremediation: Targeted removal of heavy metals, hydrocarbons, and persistent pollutants. *Environmental Sciences Europe* 2025; **37(1)**, 85.

[2] MM El-Sheekh, HY El-Kassas and SS Ali. Microalgae-based bioremediation of refractory pollutants: An approach towards environmental sustainability. *Microbial Cell Factories* 2025; **24(1)**, 19.

[3] L Liu, Z Chen, J Zhang, D Shan, Y Wu, L Bai and B Wang. Treatment of industrial dye wastewater and pharmaceutical residue wastewater by advanced oxidation processes and its combination with nanocatalysts: A review. *Journal of Water Process Engineering* 2021; **42**, 102122.

[4] SS Shetty, D Deepthi, S Harshitha, S Sonkusare, PB Naik and H Madhyastha. Environmental pollutants and their effects on human health. *Heliyon* 2023; **9(9)**, e19602.

[5] J Awewomom, F Dzeble, YD Takyi, WB Ashie, ENYO Ettey, PE Afua, LNA Sackey, F Opoku and O Akoto. Addressing global environmental pollution using environmental control techniques: A focus on environmental policy and preventive environmental management. *Discover Environment* 2024; **2(1)**, 8.

[6] MS Akhtar, S Ali and W Zaman. Innovative adsorbents for pollutant removal: Exploring the latest research and applications. *Molecules* 2024; **29(18)**, 4317.

[7] J Bai, X Zhang, C Wang, X Li, Z Xu, C Jing, T Zhang and Y Jiang. The adsorption-photocatalytic synergism of LDHs-based nanocomposites on the removal of pollutants in aqueous environment: A critical review. *Journal of Cleaner Production* 2024; **436**, 140705.

[8] S Khan, T Noor, N Iqbal and L Yaqoob. Photocatalytic dye degradation from textile wastewater: A review. *ACS* Omega 2024; **9(20)**, 21751-21767.

[9] S Mishra and B Sundaram. A review of the photocatalysis process used for wastewater treatment. *Materials Today: Proceedings* 2024; **102**, 393-409.

[10] K Derkaoui, I Bencherifa, A Elfiad, Y Mebdoua, I Belkhettab, K Boukhouidem, S Benredouane, T Hadjersi, A Manseri and M Kechouane. Unveiling the optical and dielectric properties of $MnFe_2O_4$: A high-performance visible-light photocatalyst for sustainable rhodamine B degradation. *Journal of Electronic Materials* 2025; **54(1)**, 5271-5286.

[11] JAL Medina, D Domínguez, P Pizá, G Liu, C Velez, FR Gómez, MH Farías, U Caudillo-Flores, GS Herrera, H Tiznado and JR Mejía-Salazar. Magnetic photocatalyst nanocomposite based on $MnFe_2O_4$@ZnO for AZO Dye Degradation. *ACS Omega* 2025; **10**, 17595-17610.

[12] Y Han, X Li, N Fu, J He, X Li, G Teng and C Zhang. Design of a hollow $MnFe_2O_4$@C@graphdiyne heterostructure for enhanced visible-light photocatalysis of tetracycline hydrochloride. *Journal of Photochemistry and Photobiology A: Chemistry* 2026; **470**, 116644.

[13] Y Li, Y Dai, L Cai, S Yang, J Wang, B Liu, X Ding, YF Zhang, Y Li, C Lu and L Wan. Efficient adsorption and photocatalytic degradation of organic dyes by novel chitosan/polyaniline/$MnFe_2O_4$ composites. *Journal of Molecular Liquids* 2025; **424**, 126995.

[14] X Ren, Y Wang, Z Pan, Q Lu, Q Guo, D Gao, P Huang, W Zhang, L Wang and X Hu. Natural sepiolite supported $MnFe_2O_4$ as an efficient peroxymonosulfate catalyst for tetracycline degradation: Performance, mechanism and degradation pathway. *Journal of Water Process Engineering* 2024; **68**, 106537

[15] MF Lanjwani, M Tuzen, MY Khuhawar and TA Saleh. Trends in photocatalytic degradation of organic dye pollutants using nanoparticles: A review. *Inorganic Chemistry Communications* 2024; **159**, 111613.

[16] MS Amulya, HP Nagaswarupa, MA Kumar, CR Ravikumar and KB Kusuma. Sonochemical synthesis of $MnFe_2O_4$ nanoparticles and their electrochemical and photocatalytic properties. *Journal of Physics and Chemistry of Solids* 2021; **148**, 109661.

[17] ZU Zango, A Garba, A Haruna, SS Imam, AU Katsina, AF Ali, AZ Abidin, MU Zango, ZN Garba, A Hosseini-Bandegharaei, AU Yuguda and H Adamu. A systematic review on applications of biochar and activated carbon derived from biomass as adsorbents for sustainable remediation of antibiotics from pharmaceutical wastewater. *Journal of Water Process Engineering* 2024; **67**, 106186.

[18] J Hemalatha, M Senthil, D Madhan, AM Al-Mohaimeed and WA Al-onazi. Fabrication of $NiFe_2O_4$ nanoparticles loaded on activated carbon as novel composites for high efficient ultra violet-light photocatalysis for degradation of aqueous organic pollutants. *Diamond and Related Materials* 2024; **144**, 110995.

[19] M Gayathiri, T Pulingam, KT Lee and K Sudesh. Activated carbon from biomass waste precursors: Factors affecting production and adsorption mechanism. *Chemosphere* 2022; **294**, 133764.

[20] M Mariana, AK Hps, EM Mistar, EB Yahya, T Alfatah, M Danish and M Amayreh. Recent advances in activated carbon modification techniques for enhanced heavy metal adsorption. *Journal of Water Process Engineering* 2021; **43**, 102221.

[21] D Dey, T Shafi, S Chowdhury, BK Dubey and R Sen. Progress and perspectives on carbon-based materials for adsorptive removal and photocatalytic degradation of perfluoroalkyl and polyfluoroalkyl substances (PFAS). *Chemosphere* 2024; **351**, 141164.

[22] LH Bao, XT Nguyen, TTH Hang, MC Vu, DT Nguyen and TN Thi. Effective adsorptive removal of pentachlorophenol in water using magnetical manganese ferrite nanoparticles immobilized on domestic activated carbon. *Journal of Technology and Science Training* 2024; **37(4)**, 28-36.

[23] HB Le, KT Nguyen, TX Nghiem, BQ Nguyen, CTH Nguyen, CN Pham, TK Nguyen and NN Dao. Efficient photocatalytic remediation of persistent organic pollutants using magnetically recoverable spinel manganese ferrite nanoparticles supported on activated carbon. *Materials Research Bulletin* 2024; **178**, 112913.

[24] H Qin, Y He, P Xu, D Huang, Z Wang and H Wang. Spinel ferrites (MFe_2O_4): Synthesis, improvement and catalytic application in environment and energy field. *Advances in Colloid and Interface Science* 2021; **294**, 102486.

[25] AR Liandi, AH Cahyana, AJF Kusumah, A Lupitasari, DN Alfariza, R Nuraini, RW Sari and FC Kusumasari. Recent trends of spinel ferrites (MFe_2O_4: Mn, Co, Ni, Cu, Zn) applications as an environmentally friendly catalyst in multicomponent reactions: A review. *Case Studies in Chemical and Environmental Engineering* 2023; **7**, 100303.

[26] B Boukoussa, KR Cherdouane, R Zegai, A Mokhtar, M Hachemaoui, I Issam, J Iqbal, SP Patole, FZ Zeggai, R Hamacha and M Abboud. Preparation of activated carbon-metal nanoparticle composite materials for the catalytic reduction of organic pollutants. *Surfaces and Interfaces* 2024; **44**, 103622.

[27] JM Gonçalves, LV de Faria, AB Nascimento, RL Germscheidt, S Patra, LP Hernández-Saravia, JA Bonacin, RAA Munoz and L Angnes. Sensing performances of spinel ferrites MFe_2O_4 (M = Mg, Ni, Co, Mn, Cu and Zn) based electrochemical sensors: A review. *Analytica Chimica Acta* 2022; **1233**, 340362.

[28] S Sharifi, K Rahimi and A Yazdani. Highly improved supercapacitance properties of $MnFe_2O_4$ nanoparticles by MoS2 nanosheets. *Scientific Reports* 2021; **11(1)**, 8378.

[29] Hakami, O. (2024). Structural, dielectric and magnetic properties of $MnFe_2O_4$/MWCNTs based nanocomposites for technological applications. *Scientific Reports* 2021; **11(1)**, 8378.

[30] OE Cigarroa-Mayorga. Tuning the size stability of $MnFe_2O_4$ nanoparticles: Controlling the morphology and tailoring of surface properties under the hydrothermal synthesis for functionalization with myricetin. *Ceramics International* 2021; **47(22)**, 32397-32406.

[31] C Simon, A Blösser, M Eckardt, H Kurz, B Weber, M Zobel and R Marschall. Magnetic properties and structural analysis on spinel $MnFe_2O_4$ nanoparticles prepared via non-aqueous microwave synthesis. *Zeitschrift fur anorganische und allgemeine Chemie* 2021; **647(22)**, 2061-2072.

[32] H Mohammmadi-Manesh, S Shahidizandi and MM Loghavi. chemical co-precipitation synthesis of manganese ferrite ($MnFe_2O_4$) and evaluation of its applications in copper removal from aqueous solutions. *Journal of Nanostructures* 2023; **13(1)**, 16-28.

[33] Y Chen, F Xu, H Li, Y Li, Y Liu, Y Chen, M Li, L Li, H Jiang and L Chen. Simple hydrothermal synthesis of magnetic $MnFe_2O_4$-sludge biochar composites for removal of aqueous Pb^{2+}. *Journal of Analytical and Applied Pyrolysis* 2021; **156**, 105173.

[34] B Zhang, M Mei, K Li, J Liu, T Wang, S Chen and J Li. One-pot synthesis of $MnFe_2O_4$ functionalized magnetic biochar by the sol-gel pyrolysis method for diclofenac sodium removal. *Journal of Cleaner Production* 2022; **381**, 135210.

[35] A Manohar, C Krishnamoorthi, C Pavithra and N Thota. Magnetic hyperthermia and photocatalytic properties of $MnFe_2O_4$ nanoparticles synthesized by solvothermal reflux method. *Journal of Superconductivity and Novel Magnetism* 2021; **34(1)**, 251-259.

[36] H Madhu and SR Prasad. Clay incorporated $MnFe_2O_4$ synthesized via green method for photocatalysis and antioxidant studies. *Journal of Alloys and Compounds Communications* 2025; **6**, 100062.

[37] M Sharma, A Sharma, S Kumar, J Kaur, MW Alam, HH Almutairi, SA Ansari and MM Ahmad. Eco-friendly synthesis of $MnFe_2O_4$ nano-ferrites with azadirachta indica leaf extract: Investigating structural, magnetic, and antibacterial properties. *Journal of Nanoelectronics and Optoelectronics* 2024; **19(10)**, 1022-1028.

[38] T Dippong, EA Levei and O Cadar. Recent advances in synthesis and applications of MFe_2O_4 (M= Co, Cu, Mn, Ni, Zn) nanoparticles. *Nanomaterials* 2021; **11(6)**, 1560.

[39] Z Liu, G Chen, X Li and X Lu. Removal of rare earth elements by $MnFe_2O_4$ based mesoporous adsorbents: Synthesis, isotherms, kinetics, thermodynamics. *Journal of Alloys and Compounds* 2021; **856**, 158185.

[40] R Rajalakshmi and N Ponpandian. Morphological design of $MnFe_2O_4$ facets (cube, flakes and capsules) for their role in electrical, magnetic and photocatalytic activity. *Materials Research Bulletin* 2023; **164**, 112242.

[41] G Yuan, K Li, J Zhang, H Wang, Z Huang, F Li, H Zhang, Q Jia and S Zhang. Myrica Rubra-like

$MnFe_2O_4$ Microsphere: A high efficiency microwave reduction catalyst for Cr (VI) removal from water. *Separation and Purification Technology* 2022; **286**, 120434.

[42] TDH Nguyen, MF Lin and WD Hsu. Investigations on electronic, magnetic, and optical properties of $MnFe_2O_4$ through first-principles calculations. *Computational Materials Science* 2024; **235**, 112831.

[43] X Jiang, S Zhao, Y Qi, J Zhang, W Liu, Q Zhao and Y Shen. Synthesis of a halloysite/$MnFe_2O_4$ heterogeneous Fenton catalyst for the efficient degradation of organic pollutants. *International Journal of Minerals, Metallurgy and Materials* 2025; **32(5)**, 1270-1282.

[44] D Deivatamil, JAM Mark, T Raghavan and JP Jesuraj. Fabrication of $MnFe_2O_4$ and Ni: $MnFe_2O_4$ nanoparticles for ammonia gas sensor application. *Inorganic Chemistry Communications* 2021; **123**, 108355.

[45] R Mazurenko, S Prokopenko, M Godzierz, A Hercog, S Makhno, U Szeluga, P Gorbyk, B Trzebicka and M Kartel. Synthesis of nanosized spinel ferrites $MnFe_2O_4$ on the surface of carbon nanotubes for the creation of polymer composites with enhanced microwave absorption capacity. *Applied Materials Today* 2023; **35**, 101972.

[46] M Tang, Y Zou, Z Jiang, P Ma, Z Zhou, X Zhu, J Bao and SG Sun. Healing the structural defects of spinel $MnFe_2O_4$ to enhance the electrocatalytic activity for oxygen reduction reaction. *Journal of Energy Chemistry* 2024; **97**, 12-19.

[47] S Bhat, UT Uthappa, T Sadhasivam, T Altalhi, SS Han and MD Kurkuri. Abundant cilantro derived high surface area activated carbon (AC) for superior adsorption performances of cationic/anionic dyes and supercapacitor application. *Chemical Engineering Journal* 2023; **459**, 141577.

[48] YX Gan. Activated carbon from biomass sustainable sources. *C* 2021; **7(2)**, 39.

[49] S Ullah, SSA Shah, M Altaf, I Hossain, ME El Sayed, M Kallel, ZM El-Bahy, A Rehman, T Najam and MA Nazir. Activated carbon derived from biomass for wastewater treatment: Synthesis, application and future challenges. *Journal of Analytical and Applied Pyrolysis* 2024; **179**, 106480.

[50] K Kanjana, P Harding, T Kwamman, W Kingkam and T Chutimasakul. Biomass-derived activated carbons with extremely narrow pore size distribution via eco-friendly synthesis for supercapacitor application. *Biomass and Bioenergy* 2021; **153**, 106206.

[51] EH Sujiono, D Zabrian, V Zharvan and NA Humairah. Fabrication and characterization of coconut shell activated carbon using variation chemical activation for wastewater treatment application. *Results in Chemistry* 2022; **4**, 100291.

[52] K Malini, D Selvakumar and NS Kumar. Activated carbon from biomass: Preparation, factors improving basicity and surface properties for enhanced CO_2 capture capacity-A review. *Journal of CO_2 Utilization* 2023; **67**, 102318.

[53] I Demiral, C Samdan and H Demiral. Enrichment of the surface functional groups of activated carbon by modification method. *Surfaces and Interfaces* 2021; **22**, 100873.

[54] I Neme, G Gonfa and C Masi. Activated carbon from biomass precursors using phosphoric acid: A review. *Heliyon* 2022; **8(12)**, e11940.

[55] J Li, W Zhou, J Li, N Xue, X Meng, L Xie, Y Yu, Z Liu, Z Qu, J Gao, F Sun and G Zhao. Efficient production of activated carbon with well-developed pore structure based on fast pyrolysis-physical activation. *Journal of the Energy Institute* 2024; **115**, 101685.

[56] F Mbarki, T Selmi, A Kesraoui and M Seffen. Low-cost activated carbon preparation from Corn stigmata fibers chemically activated using H_3PO_4, $ZnCl_2$ and KOH: Study of methylene blue adsorption, stochastic isotherm and fractal kinetic. *Industrial Crops and Products* 2022; **178**, 114546.

[57] G Zhang, H Yang, M Jiang and Q Zhang. Preparation and characterization of activated carbon derived from deashing coal slime with $ZnCl_2$ activation. *Colloids and Surfaces A: Physicochemical and Engineering Aspects* 2022; **641**, 128124.

[58] JM Illingworth, B Rand and PT Williams. Understanding the mechanism of two-step, pyrolysis-alkali chemical activation of fibrous biomass for the production of activated carbon

fibre matting. *Fuel Processing Technology* 2022; **235**, 107348.

[59] R Zou, Z Yang, J Zhang, R Lei, W Zhang, F Fnu, DCW Tsang, J Heyne, X Zhang, R Ruan and H Lei. Machine learning application for predicting key properties of activated carbon produced from lignocellulosic biomass waste with chemical activation. *Bioresource Technology* 2024; **399**, 130624.

[60] MO Prakash, G Raghavendra, S Ojha and M Panchal. Characterization of porous activated carbon prepared from arhar stalks by single step chemical activation method. *Materials Today: Proceedings* 2021; **39**, 1476-1481.

[61] SC Hu, J Cheng, WP Wang, GT Sun, LL Hu, MQ Zhu and XH Huang. Structural changes and electrochemical properties of lacquer wood activated carbon prepared by phosphoric acid-chemical activation for supercapacitor applications. *Renewable Energy* 2021; **177**, 82-94.

[62] R Ganjoo, S Sharma, A Kumar and MM Daouda. *Activated carbon: Fundamentals, classification, and properties. In*: C Verma and MA Quraishi (Eds.). Activated carbon: Progress and applications. The Royal Society of Chemistry, London, 2023.

[63] G Sharma, S Sharma, A Kumar, CW Lai, M Naushad, Shehnaz, J Iqbal and FJ Stadler. Activated carbon as superadsorbent and sustainable material for diverse applications. *Adsorption Science & Technology* 2022; **2022**, 4184809.

[64] S Zhang, M Zheng, Y Tang, R Zang, X Zhang, X Huang, Y Chen, Y Yamauchi, S Kaskel and H Pang. Understanding synthesis-structure-performance correlations of nanoarchitectured activated carbons for electrochemical applications and carbon capture. *Advanced Functional Materials* 2022; **32(40)**, 2204714.

[65] MA Hadj Ammar, B Benhaoua and K Salhi. Performance study and advantages of a novel activated carbon adsorption cycle run by sunlight. *Arabian Journal for Science and Engineering* 2021; **46**, 5933-5944.

[66] JB Park, DW Lee, CH Lee, YS Hong and JK Suh. Manufacturing of spherical activated carbons using anion exchange resins and analysis of the properties. *Research Square* 2024. https://doi.org/10.21203/rs.3.rs-3954210/v1

[67] M Gayathiri, T Pulingam, KT Lee and K Sudesh. Activated carbon from biomass waste precursors: Factors affecting production and adsorption mechanism. *Chemosphere* 2022; **294**, 133764.

[68] M Mariana, AK Hps, EM Mistar, EB Yahya, T Alfatah, M Danish and M Amayreh. Recent advances in activated carbon modification techniques for enhanced heavy metal adsorption. *Journal of Water Process Engineering* 2021; **43**, 102221.

[69] N Abuelnoor, A AlHajaj, M Khaleel, LF Vega and MR Abu-Zahra. Activated carbons from biomass-based sources for CO_2 capture applications. *Chemosphere* 2021; **282**, 131111.

[70] M Lewoyehu. Comprehensive review on synthesis and application of activated carbon from agricultural residues for the remediation of venomous pollutants in wastewater. *Journal of Analytical and Applied Pyrolysis* 2021; **159**, 105279.

[71] S Ullah, SSA Shah, M Altaf, I Hossain, ME El Sayed, M Kallel, ZM El-Bahy, A Rehman, T Najam and MA Nazir. Activated carbon derived from biomass for wastewater treatment: Synthesis, application and future challenges. *Journal of Analytical and Applied Pyrolysis* 2024; **179**, 106480.

[72] X Wang, H Cheng, G Ye, J Fan, F Yao and Y Wang. Key factors and primary modification methods of activated carbon and their application in adsorption of carbon-based gases: A review. *Chemosphere* 2022; **287**, 131995.

[73] P Vijuksungsith, T Satapanajaru, C Chokejaroenrat, C Jarusutthirak, C Sakulthaew, A Kambhu, M Yoo-iam and R Boonprasert. Removal and reuse of phosphorus from aquaculture water using activated carbon-based CaO_2 nanoparticles. *Environmental Technology & Innovation* 2023; **29**, 102990.

[74] Y Cao, Y Jin, Z Zhou, S Tian and Z Ren. Magnetic catalysts of $MnFe_2O_4$-AC activated peroxydisulfate for high-efficient treatment of norfloxacin wastewater. *Chemical Physics Letters* 2024; **840**, 141159.

[75] Y Wang, C Lin, X Liu, W Ren, X Huang, M He and W Ouyang. Efficient removal of acetochlor pesticide from water using magnetic activated carbon: Adsorption performance, mechanism, and regeneration exploration. *Science of the Total Environment* 2021; **778**, 146353.

[76] HM Sabaa, KM El-Khatib, MY El-Kady and SA Mahmoud. Spinel structure of activated carbon supported MFe_2O_4 composites as an economic and efficient electrocatalyst for oxygen reduction reaction in neutral media. *Journal of Solid State Electrochemistry* 2022; **26(12)**, 2749-2763.

[77] NTH Nguyen, GT Tran, TTT Nguyen, DTC Nguyen and T Van Tran. Synthesis of $MnFe_2O_4$/activated carbon derived from durian shell waste for removal of indole in water: Optimization, modelling, and mechanism. *Environmental Research* 2024; **254**, 118883.

[78] TT Do, TH Nguyen, TD Nguyen and HT Van. The ammonium adsorption capacity of coffee husk-derived activated carbon composite with $MnFe_2O_4$. *HPU2 Journal of Sciences: Natural Sciences and Technology* 2025; **04**, 39-47.

[79] A Ashfaq, MZ Ashfaq, X Cheng, H Gong, A Saleem and R Iqbal. Coconut shell waste encased $MnFe_2O_4$ for enhanced microwave absorption. *Journal of Alloys and Compounds* 2024; **1002**, 175116.

[80] F Riyanti, PL Hariani, W Purwaningrum, Elfita, SS Damarril and I Amelia. The synthesis of $MnFe_2O_4$-activated carbon composite for removal of methyl red from aqueous solution. *Molekul* 2018; **13(2)**, 123-132.

[81] SJ Salih and WM Mahmood. Review on magnetic spinel ferrite (MFe_2O_4) nanoparticles: From synthesis to application. *Heliyon* 2023; **9(6)**, e16601.

[82] Y Sun, J Feng, W Zhu, R Hou, B Zhang and A Ishag. The recent advances of $MnFe_2O_4$-based nanoparticles in environmental application: A review. *Science of the Total Environment* 2024; **954**, 176378.

[83] Y Tang, S Yang, L Dong, W Xie, X Yi and H Gu. Magnetic amorphous carbon@ manganese ferrite hybrid materials as a heterogeneous persulfate activator for catalytic oxidation of tetrabromobisphenol A. *Separation and Purification Technology* 2022; **303**, 122230.

[84] AG Niculescu, B Mihaiescu, D Mihaiescu, T Hadibarata and A Grumezescu. An updated overview of magnetic composites for water decontamination. *Polymers* 2024; **16**, 709.

[85] HM Sabaa, KM El-Khatib, MY El-Kady and SA Mahmoud. Spinel structure of activated carbon supported MFe_2O_4 composites as an economic and efficient electrocatalyst for oxygen reduction reaction in neutral media. *Journal of Solid State Electrochemistry* 2022; **26**, 2749-2763.

[86] X Xie, B Wang, Y Wang, C Ni, X Sun and W Du. Spinel structured MFe_2O_4 (M = Fe, Co, Ni, Mn, Zn) and their composites for microwave absorption: A review. *Chemical Engineering Journal* 2022; **428**, 131160.

[87] Intensify mass transfer and molecular oxygen activation by defect-bridged asymmetric catalytic sites toward efficient membrane-based nanoconfined catalysis. *Advanced Functional Materials* 2024; **34(37)**, 2403964.

[88] CM Manivel, ALT Zheng, R Kannan, S Seenivasagam, TY Yun Hin, S Boonyuen, J Lease, Y Andou and KB Tan. ZIF-8/graphene composite for photocatalytic degradation under low intensity UV irradiation and antibacterial applications. *Scientific Reports* 2025; **15**, 33875.

[89] M Long, D Li, H Li, X Ma, Q Zhao, Q Wen and F Song. Synergetic effect of photocatalysis and peroxymonosulfate activated by MFe_2O_4 (M = Co, Mn, or Zn) for enhanced photocatalytic activity under visible light irradiation. *RSC Advances* 2022; **12**, 20946-20955.

[90] S Meng, M Sun, P Zhang, C Zhou, C He, H Zhang, Y Liu, Z Xiong, P Zhou and B Lai. Metal borides as excellent co-catalysts for boosted and long-lasting fenton-like reaction: Dual co-catalytic centers of metal and boron. *Environmental Science & Technology* 2023; **57(33)**, 12534-12545.

[91] Z Yang, C Shan, JJ Pignatello and B Pan. Mn (II) acceleration of the picolinic acid-assisted Fenton reaction: New insight into the role of manganese in homogeneous Fenton AOPs. *Environmental Science & Technology* 2022; **56(10)**, 6621-6630.

[92] W Zhao and B Yang. Fabrication of magnetic $MnFe_2O_4$@ HL composites with an *in situ* Fenton-like reaction for enhancing tetracycline degradation. *Journal of Colloid and Interface Science* 2024; **658**, 997-1008.

[93] Y Zhou, Y Zhang and X Hu. Enhanced activation of peroxymonosulfate using oxygen vacancy-enriched $FeCo_2O_{4-x}$ spinel for 2,4-dichlorophenol removal: Singlet oxygen-dominated nonradical process. *Colloids and Surfaces A: Physicochemical and Engineering Aspects* 2020; **597**, 124568.

[94] K Poomipuen, C Sakulthaew, C Chokejaroenrat, A Angkaew, K Techauay, T Poompoung, K Teingtham, P Phansak, P Lueangjaroenkit and DD Snow. Dual activation of peroxymonosulfate using $MnFe_2O$/g-C_3N_4 and visible light for the efficient degradation of steroid hormones: performance, mechanisms, and environmental impacts. *ACS Omega* 2023; **8(39)**, 36136-36151.

[95] Y Liang, R Tao, B Zhao, Z Meng, Y Cheng, F Yang, H Lei and L Kong. Roles of iron and manganese in bimetallic biochar composites for efficient persulfate activation and atrazine removal. *Biochar* 2024; **6(1)**, 41.

[96] S Xu, L Wen, C Yu, S Li and J Tang. Activation of peroxymonosulfate by $MnFe_2O_4$@BC composite for bisphenol A degradation: The coexisting of free-radical and non-radical pathways. *Chemical Engineering Journal* 2022; **442**, 136250.

[97] XL Chen, H Li, LH Lai, YX Zhang, Y Chen, XK Li, B Liu and HJ Wang. Peroxymonosulfate activation using $MnFe_2O_4$ modified biochar for organic pollutants degradation: Performance and mechanisms. *Separation and Purification Technology* 2023; **308**, 122886.

[98] Y Sun, F Liu, Y Gao, J Dou, Y Jiang, A Deng, L Zhao and H Liu. Flower-Shaped $MnFe_2O_4$@MoS_2 Nanocomposite Activated H_2O_2 for efficient degradation of tetracycline: Performance evaluation, mechanism and degradation pathway. *Catalysts* 2024; **14(10)**, 738.

[99] S Noor, A Ashar, MB Taj and ZA Bhutta. *Advanced oxidation processes for remediation of persistent organic pollutants. In*: MP Shah, SP Bera and GY Tore (Eds.). Advanced oxidation processes for wastewater treatment. 1st ed. CRC Press, Boca Raton, United States, 2022, p. 203-212.

[100] J Wang, X Xu, Z Peng, G Kuang, W Ke, H Wang, W Lv, S Zhan, Y Li and Z Zhang. Enhancing reactive oxygen species generation and pollutant adsorption in advanced oxidation processes with cation vacancy-driven dual-site Mn_2SiO_4 ctalysts. *Advanced Materials* 2026; **38(2)**, e13231.

[101] AC Unnikrishnan, BK Das, P Saveri, E Mani, AP Deshpande and G Shanmugam. efficiency enhancement in peptide hydrogelators: The crucial role of side chain hydrogen bonding over aromatic pi-pi interactions. *Langmuir* 2024; **40**, 24405-24418.

[102] AA Ahmad, A Alwahbi, LA Al Khatib and H Dammag. *Biomass-based activated carbon. In*: E Jacob-Lopes, LQ Zepka and RR Dias (Eds.). From biomass to biobased products. IntechOpen, London, 2024.

[103] XL Chen, H Li, LH Lai, YX Zhang, Y Chen, XK Li, B Liu and HJ Wang. Peroxymonosulfate activation using $MnFe_2O_4$ modified biochar for organic pollutants degradation: Performance and mechanisms. *Separation and Purification Technology* 2023; **308**, 122886.

[104] X Jiang, Z Tan, G Jiang, C Liu, G Gao and Z Liu. Novel magnetic $MnFe_2O_4$-decorated graphite-like porous biochar as a heterogeneous catalyst for activation of peroxydisulfate toward degradation of rhodamine B. *ACS Omega* 2024; **9**, 6455-6465.

[105] RR Bhosale, S Akhter, RB Gupta and RV Shende. Utilization of $MnFe_2O_4$ redox ferrite for solar fuel production via CO_2 splitting: A thermodynamic study. *Energies* 2023; **16**, 5479.

[106] H Qin, Y He, P Xu, D Huang, Z Wang, H Wang, Z Wang, Y Zhao, Q Tian and C Wang. Spinel ferrites (MFe_2O_4): Synthesis, improvement and catalytic application in environment and energy field. *Advances in Colloid and Interface Science* 2021; **294**, 102486.

[107] L Ndlwana, R Naledi, KM Dimpe, HF Ogutu, EO Oseghe, MM Motsa, TAM Msagati and BB Mamba. Sustainable hydrothermal and solvothermal synthesis of advanced carbon materials in multidimensional applications: A review. *Materials* 2021; **14(17)**, 5094.

[108] Z Fallah, EN Zare, M Ghomi, F Ahmadijokani, M Amini, M Tajbakhsh, M Arjmand, G Sharma, H Ali, A Ahmad, P Makvandi, E Lichtfouse, M Sillanpaa and RS Varma. Toxicity and remediation of pharmaceuticals and pesticides using metal oxides and carbon nanomaterials. *Chemosphere* 2021; **275**, 130055.